UILU-ENG-95-2558

INTAKE TUNING, ETHANOL CONVERSION, AND EMISSIONS ANALYSIS OF A 620 cc FOUR STROKE V-TWIM ENGINE

PHILIP ROBERT GUZIEC

Power Affiliates Program

Department of Electrical and Computer Engineering

University of Illinois at Urbana-Champaign

Urbana, Illinois 61801

PAP-TR-95-9

August 1995

FOREWARD

This technical report is a reprint of the thesis written by Philip Robert Guziec as partial fulfillment of the requirements for the degree of Master of Science in Mechanical Engineering at the University of Illinois.

Robert White

Thesis Advisor

August 1995

Acknowledgements

To Professor White, for your guidance and assistance throughout my undergraduate and graduate education, thank you. To Leland McWhorter, I appreciate your patience and hard work in fabricating the intake manifold. To Peter Nelson, your considerable help with my fuel injection computer design and programming was invaluable. To Tim Frazier, I appreciate your assistance in using the emissions analysis equipment under your care. To my parents, for your support and encouragement, thank you. Finally, I would like to thank both my parents and my advisor for their tolerance of the duration of my research and writing.

Table of Contents

1.0 Introduction

Acceleration and hill climbing power requirements of a typical United States passenger vehicle normally dictate the required peak power for the selection of the vehicle's engine. The equation for the power required by a vehicle is as follows:

$$\text{Power(hp)} = \{C_r M_v g + M_v[a + g*\sin(\text{theta})] + .5(\text{rho}) C_d A_v S_v^2\} S_v/550 \quad (1.1)$$

Where:
- C_r = coefficient of rolling resistance [lbf/lbf]
- M_v = mass of vehicle [slugs]
- g = acceleration of gravity [ft/s^2]
- a = acceleration of vehicle [ft/s^2]
- theta = angle of incline of road
- rho = density of air [$slug/ft^3$]
- C_d = drag coefficient of vehicle
- A_v = frontal area of vehicle [ft^2]
- S_v = speed of vehicle [ft/sec]

It is interesting to note that the additional power required due to the component of gravitational acceleration of an inclined road acting directly against the vehicle's motion is indistinguishable from the additional power required due to accelerations of the vehicle. Due to low maximum speed limits in the U.S., the conditions above lead to engines that are typically sized to produce far more power than what is required by the vehicle at normal cruising speeds. For example, a typical 3500 lb vehicle with a C_r of .012, a 21 ft^2 frontal area with a C_d of .34 traveling at 60 mph on a level road requires only 12.7 kW (16.6 hp) while an acceleration of .1 g requires an additional 41.7 kW (55.9 hp) and a 5% grade requires a further 20.9 KW (28.0 hp). These transient power requirements result in an engine that is larger and heavier than needed

to supply the average power required by the vehicle, and consequently one which is run primarily under heavily throttled conditions. The engine is also mechanically connected to the drive wheels by a transmission causing any change in the power or speed requirements of the vehicle to require a corresponding change in the engine power or speed.

Series type Hybrid Electric Vehicles (HEVs) have an electric motor driving the wheels with the electric power supplied by a combination of batteries and a power source known as an Auxiliary Power Unit (APU), which converts chemical energy to electrical energy. The APU can consist of an Internal Combustion Engine (ICE) or gas turbine coupled to a generator, a fuel cell, or any other means of converting chemical energy to electrical energy. The University of Illinois selected an ICE for the HEV because it is an inexpensive well known technology which is readily available. Since there is no mechanical connection between the APU and the drive wheels, the speed and power of the APU need not directly correspond to the speed and immediate power requirements of the vehicle. This decoupling provides unique opportunities for the isolation of engine operating conditions from the transients of the road speed and power of the vehicle.

In a series type HEV, the battery pack can be chosen with a capacity to provide or store the difference between the power requirements of the vehicle and the power output of the APU. This storage capacity allows the selection of an APU which produces the overall average power required by the vehicle. In the case of an ICE powered APU, a constant power level can be selected and optimized for minimum Brake Specific Fuel Consumption (BSFC) and tailpipe emissions.

Optimization for minimum BSFC and minimum emissions are related in that minimum specific fuel consumption reduces overall emissions by reducing the quantity of fuel burned and percentage emissions are related to BSFC, as will be discussed in chapter 6. Proper selection of the generator control strategy can relieve the engine controller of the task of following rapid transients, allowing for more accurate fuel and spark control and more uniform loading of the catalyst.

Series type HEVs can also be provided with a battery pack capacity sufficient for a limited range without the APU in operation, allowing for daily short range commuting from an at home recharging station. Hybrid operation can be made completely transparent to the driver, with operation of the APU triggered automatically by an on board micro controller at a selected state of charge of the battery pack. The APU should be started near the limit of the electric range and, by estimating the rate of discharge of the battery pack, the time until APU start can be estimated. With the abundant electrical energy available from the battery pack, the APU can be prepared for starting by preheating the catalytic converter and Exhaust Gas Oxygen (EGO) sensor to operating temperature. This can provide a considerable reduction in cold start emissions[1]. The overall effect on emissions reduction can be significant, since cold start emissions account for 60% to 80% of the overall emissions of a modern automobile on the federal emissions test procedure[2]. Preheating of the catalyst and EGO sensor and starting of the APU can be controlled entirely by the on board micro controller, eliminating the delay experienced with preheated catalytic converter installations in traditional automobiles.

The engine selected for the University of Illinois hybrid electric vehicle is a Kawasaki FD 620D small industrial engine used in John Deere riding mowers. The FD 620D is a modern small industrial and off road vehicle V-twin engine designed to meet 1997 off road vehicle emissions requirements. The engine was selected for its rated power output, light weight, and emissions conscious design. The engine has an aluminum block and heads, with two pushrod activated valves per cylinder, a nominal compression ratio of 10:1, and weighs 42 kilograms. The engine as manufactured by Kawasaki is equipped with a single throttle body fuel injection system flowing into a simple two leg manifold controlled by an open loop speed-density control computer. Baseline testing showed that the system resulted in an equivalence ratio maldistribution of up to 20% between the cylinders due to the throttle plate location, the throttle plate angle, the injector inlet location, and the timing of the fuel injection pulse relative to the unevenly timed intake strokes of the two cylinders. Consequently, an intake manifold and fuel injection system was designed to replace the one supplied by the manufacturer in order to increase maximum power, reduce fuel maldistribution between the cylinders, and reduce overall emissions.

Ethanol was selected as the primary fuel for the HEV due to the potential for emissions reduction and because of its status as an alternate fuel and a renewable resource.

2.0 Theory and Design

2.1 Intake Manifold

The replacement intake manifold was designed with tuned runner length and a closed loop port fuel injection system in order to increase peak power and efficiency and reduce emissions. The system was optimized about the manufacturer's rated speed of 3600 RPM due to noise and durability considerations. Wide Open Throttle (WOT) operation was chosen as optimum for maximum power output and minimum BSFC based on testing of the engine as supplied by the manufacturer.

The intake manifold was designed to minimize intake airflow pressure losses and was tuned for peak airflow at the design RPM using Helmholtz [4] resonance theory. Individual port fuel injection was selected to minimize fuel maldistribution and allow the separation of the intake runners. Due to the uneven, 0 - 270° - 720°, firing order of the V twin engine, the intake runners for the two cylinders were kept completely separated up to the air filter. Two throttle plates were used, one in each intake runner, and a small balance tube between the runners provided equalization of intake runner pressures between the two ports at idle and a common measurement point for the manifold pressure sensor. Thus, for the purpose of this analysis, the cylinders were treated as two single cylinder engines.

The simple Helmholtz model was selected for intake tuning because it is the dominant effect in single cylinder intake tuning and can quickly and accurately predict the RPM at which the tuning peak occurs. According to Thompson and Engleman[3], "the total breathing curve is

the result of the increase in breathing due to Helmholtz type resonance with organ pipe oscillation ripples superimposed upon the Helmholtz tuning." Organ pipe contributions to the tuning effect are ignored in this analysis.

The equation for Helmholtz tuning RPM for a single inlet pipe is:

$$RPM = 162/K * C_s * \text{Sqrt}[A/(L*V_D)] * \text{Sqrt}\,[(R-1)/(R+1)] \quad (2.1)$$

Where:
- K is a constant (2.0 to 2.5) depending on valve timing
- C_s is the speed of sound in the inlet (ft/sec)
- A is intake runner area, (in^2)
- L is the length of the inlet runner from the intake valve (in)
- V_D is volumetric displacement of the cylinder (in^3)
- R is compression ratio of the engine

The effective engine cylinder volume at mid-stroke, $V_D/2*[(R+1)/(R-1)]$, is used as the volume for the Helmholtz resonator and is included in the equation and constant 1348. According to Thompson and Engleman[3], a length of pi/2 times the diameter of the runner should be added to the length to account for the portion of the free air in the mouth of the tube which moves at significant velocity. In this design, an intake bell mouth is used to prevent a vena contracta from reducing the effective area of the inlet of the intake runner. According to Thompson and Engleman[3], an intake bell mouth also serves to dampen out the organ pipe oscillations and improve the magnitude of the Helmholtz supercharge. According to Engleman[4], if an intake bell mouth is used, the end of the effective intake runner is in the bell mouth. For the calculations in this

study, the end of the intake bell mouth was used as the effective length of the runner.

Round aluminum tubing was chosen for the inlet runners for simplicity of fabrication, and an inside diameter of 1.15 inches was selected to most closely match the dimensions of the inlet port to the cylinder heads. This tubing diameter resulted in a mean intake gas velocity based on 100% volumetric efficiency of 43 ft/sec which is significantly lower than Engleman's recommended 200 ft/sec [4]. Thompson and Engleman's [3] paper on single cylinder intake tuning, however, contradictorily states that larger inlet runner areas result in greater maximum supercharge. For the purposes of this design, 43 ft/sec was accepted as a compromise required to properly match the intake runner to the intake port without an abrupt expansion of runner area and corresponding pressure drop.

For the optimum length of intake runner to fit within the space constraints of the application, it was necessary that the intake runners bend a number of times. The centerline length of the tubing bends are taken as the design length for the intake runners. The bends may result in some loss of supercharge, but should not change the RPM for maximum tuning [4]. In order to minimize pressure losses in the bends, the manifold is constructed of mandrel bent tubing of approximately constant cross sectional area in the bend.

Figure 2.1 is a plot of calculated tuning RPM vs. intake runner length using the recommended K factor of 2.1.[4] The sensitivity of tuning RPM to runner length at the design engine speed of 3600 RPM is about 70 RPM per inch change in length. This insensitivity, combined with the broad range of effect of Helmholtz resonance tuning [3] and [4],

indicates that there should be significant Helmholtz effect at the tuning RPM despite any error in calculation due to inaccuracies in the runner length due to bends, varying area of the inlet port, or choice of the valve timing factor K. Figure 2.1 shows that the theoretical tuning length is approximately 26 inches from the intake valve to the end of the bell mouth.

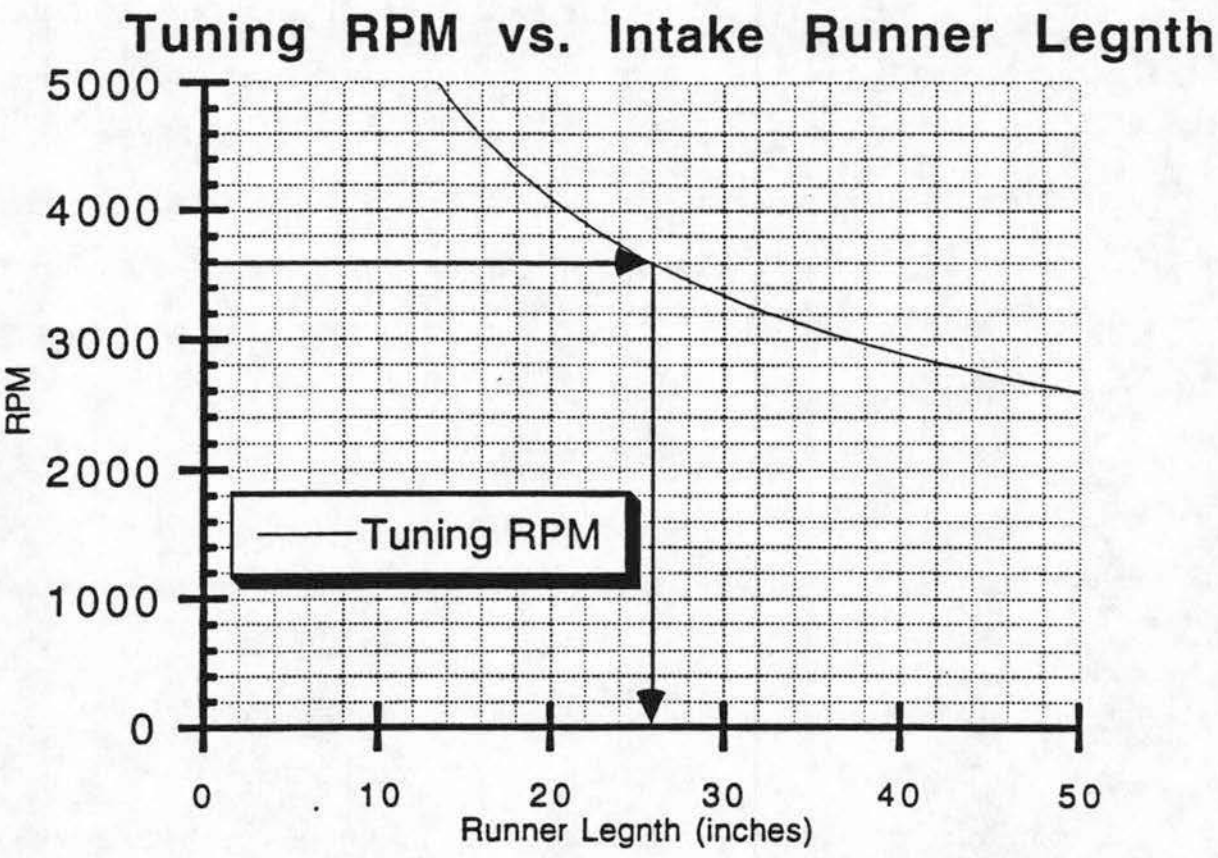

Figure 2.1

2.2 Ethanol Conversion

Using ethanol as a fuel requires an increase in fuel flow rate by a factor of 1.57 to accommodate the change in air fuel ratio from 14.6 for gasoline to 9.3 for a blend of 95% ethanol and 5% gasoline [5]. This can be accomplished by resizing the fuel injectors, increasing the fuel pressure, or increasing the pulse duration of the fuel injectors if they are of adequate size. In order to convert the throttle body intake system to ethanol operation for baseline data collection, the fuel pressure was increased to increase the fuel flow rate. When port fuel injectors were used for the new intake system, the fuel injectors were sized for the greater fuel flow rate required while still operating at the rated fuel pressure for the injectors. MBT spark timing may change due to differences in ignition delay and flame front propagation of ethanol relative to gasoline. The higher octane rating of ethanol may also allow increased spark advance if gasoline spark advance is retarded from MBT due to knock limits. Ethanol also has a much leaner flammability limit [5], allowing greater flexibility in choosing an equivalence ratio for minimum BSFC and emissions.

2.3 Operating Conditions

Modern automobile engines spend the majority of their life operating at low power levels and stoichiometric air fuel ratios. At high power levels where maximum power is a concern and emissions requirements are not applicable, the engines are run at equivalence ratios near 1.17 for both maximum power and internal engine cooling.

The test engine as supplied from the manufacturer was designed for use in a riding mower application where the primary operation would be at high load for long periods. Consequently, the engine operated at equivalence ratios of approximately 1.1 to 1.2 at all times. Operating at maximum power with stoichiometric or lean air fuel ratios is not a normal condition in either automotive engines or industrial applications of small engines, and such operation results in higher thermal loading and less internal cooling than originally accounted for in the engine design. Such high thermal loads can result in a number of wear and durability problems as well as temperature problems. These problems can include but are not limited to rapid valve seat wear, cylinder wall wear, cooling problems, and cylinder hot spots which can cause preignition. Further, ethanol does not have the lubricating effect that gasoline does, potentially exacerbating wear problems. No data was collected on the extent of these effects in the test engine.

One problem encountered in the test engine was preignition. The preignition was so severe that the engine continued to run and produce half power with the spark plugs wires disconnected. The assumed cause of the preignition was overheated spark plugs as the spark plug electrodes were completely melted away. In this instance, the problem was remedied by a change to spark plugs with a much colder heat range. Spark plug electrode problems with alcohol fuels are well known, and different materials are commonly used.

3.0 Experimental Setup

The dynamometer used for the testing was a Mid-West Dynamometer and Engineering Company eddy current type capable of absorbing a maximum of 250 horsepower. The dynamometer was controlled by a Dyne Systems Dyn-Loc digital controller using feedback from an inductive speed pick-up mounted on the dynamometer shaft and a BLH Electronics model V35B load cell. All tests were conducted at constant RPM. Constant RPM dynamometer operation closely approximates the type of continuous operation expected in a series type hybrid which buffers the engine from transient fluctuations of load and speed.

The engine was cooled by routing the coolant through a water to water heat exchanger with heat rejected to a continuously running supply of cold tap water. The flow rate was manually adjusted to maintain temperature of the coolant intake into the block between 65° C and 75° C, corresponding to the manufacturer's thermostat opening temperature of 75° C. This temperature is lower than typical modern automotive thermostats which typically operate above 95 ° C and was probably selected by the manufacturer to help reduce component temperatures during continuous high load operation.

An exhaust manifold was fabricated with two 1 inch diameter runners 18 inches in length flowing into a round chamber of 2 inch diameter and 24 inches long. This manifold was connected to the laboratory exhaust system. The exhaust backpressure was not measured during testing but was near atmospheric. The emissions

measurement samples of exhaust gases were collected with .25 inch diameter stainless tubing passing through compression fittings into the exhaust runners 2 inches from the exhaust port and bent at a small radius to a 1 inch long straight section pointing upstream at the exhaust ports. The flow was routed through heated lines to emissions measurement apparatus capable of measuring percentages of carbon monoxide, carbon dioxide, and oxygen, and PPM of unburned hydrocarbons and oxides of nitrogen. The equivalence ratio was calculated from the exhaust constituents.[4]

The fuel flow rate was measured using a calibrated burette mounted atop a sealed tank containing the high pressure fuel pump and return line from the pressure regulator. The fuel pressure regulator in conjunction with a mechanical fuel pressure gauge were used to set the fuel pressure at the 270 kPa rating of the injectors. The burette was filled prior to each measurement with a boost pump and, with the engine running at constant conditions, a stopwatch was used to measure the time required to empty the burette. This fuel measurement technique produced results repeatable within $\pm 1\%$.

Mean intake manifold pressure was measured with a mercury manometer attached to the common pressure measurement point of the intake manifold. A .007 inch metering orifice from a carburetor was used to dampen out cycle to cycle manifold pressure variations to the manometer and fuel injection system pressure sensor. Individual intake port pressure traces were measured at a tap in the intake runner wall 3 inches from the intake valve at the flange which mounted the intake manifold to the cylinder head. The pressure was measured using a Motorola MPX2200AP piezoresistive pressure sensor. The pressure

range of the sensor is 0 to 2 bar absolute with linearity within ± 0.5 percent over laboratory temperature ranges. The output voltage was amplified with an Analog Devices AMP-02 instrumentation amplifier to a final output voltage of 0 to 4 volts. The voltage was measured using an HP 54501 100 MHz digital storage oscilloscope and printed on an HP thinkjet printer. The pressure sensor was connected to the intake manifold with twelve inches of 1/8 inch ID vacuum tubing. The frequency response of the vacuum tubing and pressure sensor setup was not measured, however pressure drops at intake valve opening shown on figures 4.13 to 4.21 are vertical within the resolution of the plotter, indicating a high enough frequency response for this application.

All raw data which were collected are included in appendices 1 through 5.

4.0 Intake Manifold Tuning Results

4.1 Helmholtz Tuning Results

From the Helmholtz theory calculations, see Figure 2.1, the tuning length for Helmholtz resonance at 3600 RPM is approximately 26 inches from the intake valve to the end of the intake trumpet. To examine off design performance and to allow for the inaccuracies inherent in the K factor of the model, see section 2.1, WOT torque was measured over the effective RPM range of the engine with intake runner lengths of 18.5, 21.5, 24, and 27 inches. While varying intake runner length, the test conditions were stoichiometric equivalence ratio with ethanol fuel (E95) and the manufacturers nominal spark advance of 21 degrees. The manufacturers fuel injection computer was used to simultaneously trigger injector drivers for the two fuel injectors. Equivalence ratio was controlled by varying fuel pressure to achieve approximately .5 volts on the EGO sensor, indicating near stoichiometric operation. The imprecision inherent in this control method resulted in some scatter in the data and lower torque values than observed during later testing.

The torque data are plotted in Figure 4.1 with the vertical axis truncated to better show the effect of the different lengths. Increasing the intake runner length increases the low RPM torque and decreases the high RPM torque. The shape of the torque curve appears to be limited by the conservative camshaft timing. The intake valves do not open until Top Dead Center (TDC) and remain open for 236 degrees. Further increases in torque may be possible at the design speed with changes in valve timing.

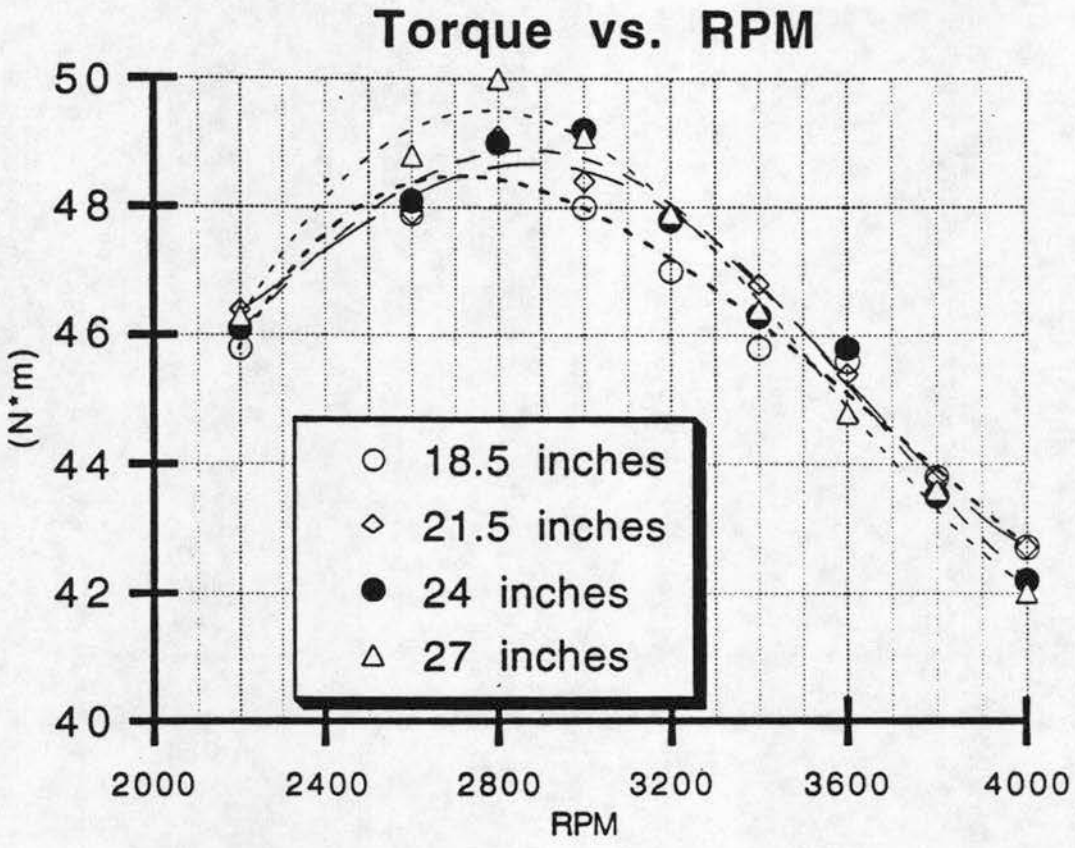

Figure 4.1

In order to show the small overall change in torque due to change in length at the design speed, torque is plotted vs. length at 3600 RPM in figure 4.2. There is a maximum at 24 inches in length, however it is barely noticeable.

An overall intake runner length of 24 inches from intake valve to bellmouth was selected based on figure 4.1 as the optimum for the design speed of 3600 RPM and all further testing was done at this length.

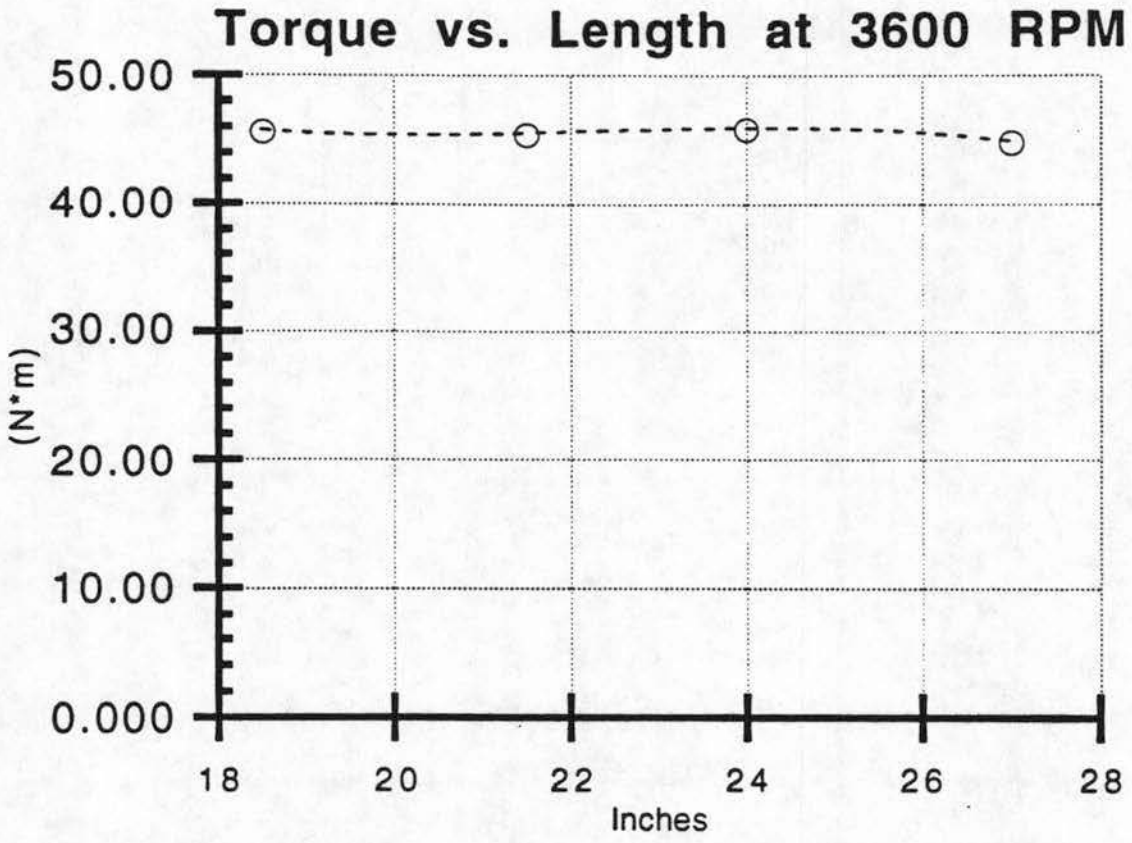

Figure 4.2

In order to compare the overall torque curve of the tuned intake manifold to that of the manufacturer's manifold, torque as a function of RPM for the tuned manifold was estimated from the data of figure 4.1. The correction was necessary to account for the increase in torque observed during later testing due to optimized spark advance and fuel control. This correction was made by multiplying the torque values in figure 4.1 at 24 inches length by the ratio of torque value observed during later testing at 3600 RPM to the value in figure 4.1 at 3600 RPM.

This estimation technique may result in inaccuracies in the estimated torque curve. As can be seen in figure 4.3, the change in the estimated peak torque RPM is small, from 2400 with the manufacturer's manifold to 2800 with the tuned manifold, but the change in shape and magnitude of the torque curve due to the tuned manifold is significant. A significant increase in maximum torque with the tuned manifold over the manufacturer's manifold was estimated, with an experimentally measured increase of 28% from 40.5 to 51.9 N*m at the design speed of 3600 RPM. This increase in torque appears to be relatively independent of tuning length, over the lengths tested, and may be partly attributable

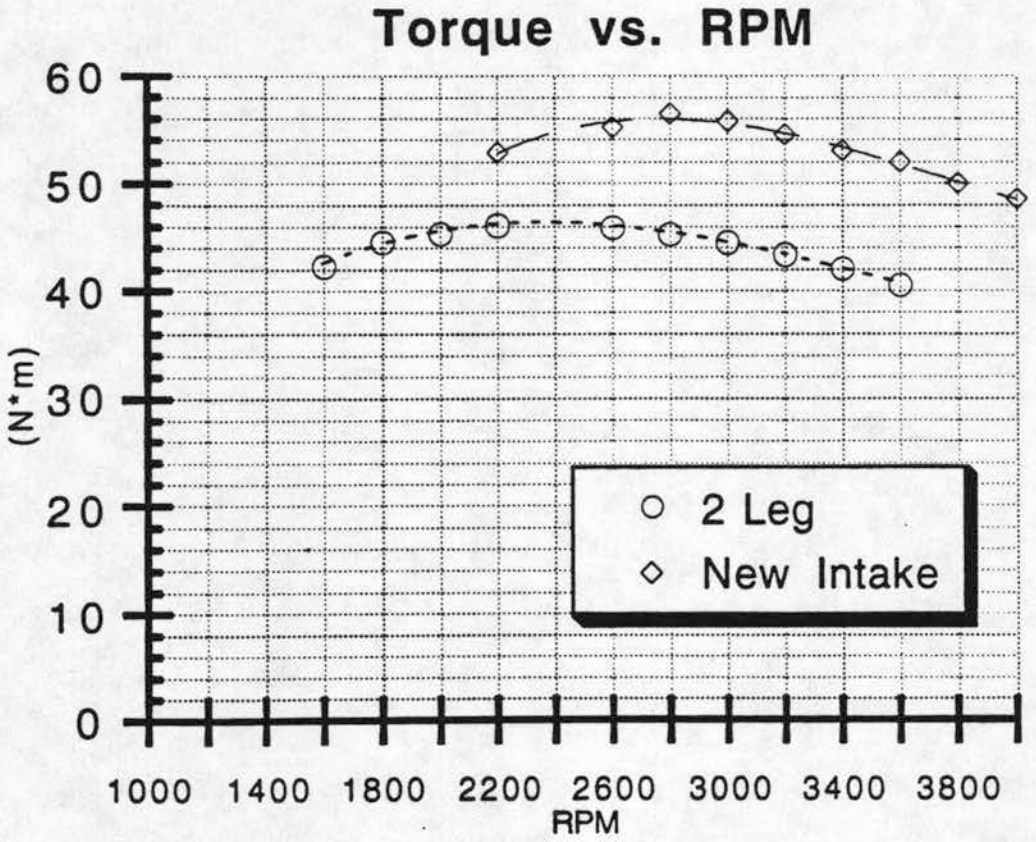

Figure 4.3

to reduced pressure losses in the intake system and more uniform fuel distribution as well as to the tuning effect. The volumetric efficiency of was calculated from BSFC, power, speed, and air fuel ratio to be 90% at 3600 RPM.

Intake manifold pressure data versus time were gathered at WOT at varying RPM to verify the existence and proper application of the Helmholtz resonance effect. The manifold pressure was measured at the intake runner wall three inches from the intake valve at the interface between the intake manifold and intake port in the cylinder head. The results are shown in figs 4.4 through 4.8 with vertical markers at IVO and IVC and each large vertical division representing .25 bar. It can be seen in figure 4.6 that at 3600 RPM, the calculated and experimental tuning maximum, the measured pressure peaks at the same time as the intake valve closes. At lower engine speeds, the pressure peaks before intake valve closing, indicating that the resonance frequency is too high for the engine RPM and the pressure peak arrives too early. This trend continues to the point where at 2400 RPM an entire resonance period can be seen during the time that the cylinder is open. Due to mechanical design limit characteristics of the engine, the maximum engine speed is limited to 4000 RPM. At 4000 RPM the pressure also peaks before the intake valve closes. The reason for this is unknown. These results and intake port pressure plots are consistent with the data and pressure plots of Thompson and Engleman [3] and clearly verify the presence and proper application of the Helmholtz tuning effect. The resonance frequency when the intake valve is closed can be seen in figure 4.4 through 4.8 to remain independent of RPM as it is solely a function of intake runner geometry.

Intake Port Pressure at 4000 RPM and Wide Open Throttle

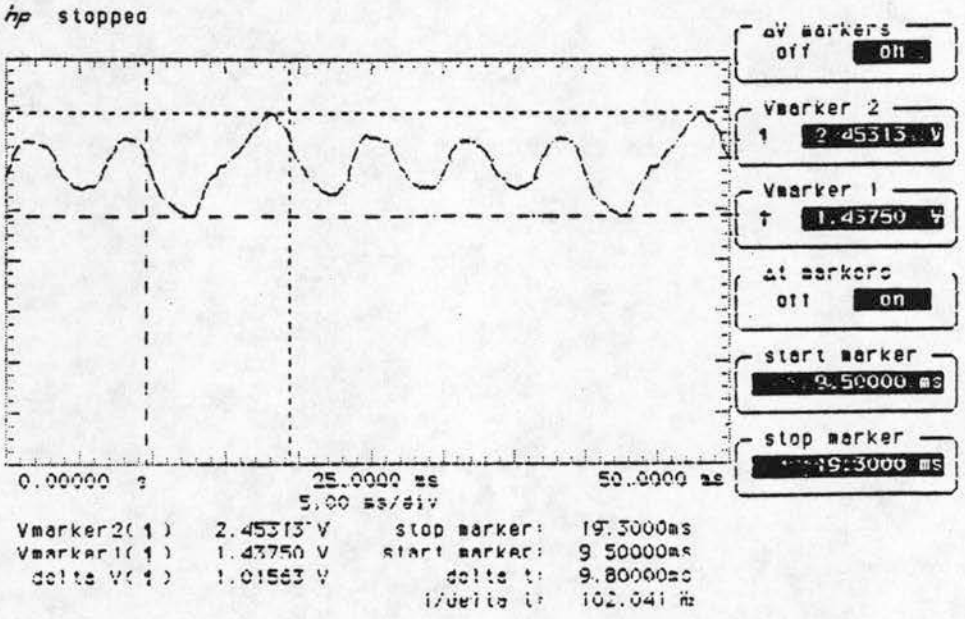

Figure 4.4

Intake Port Pressure at 3600 RPM and Wide Open Throttle

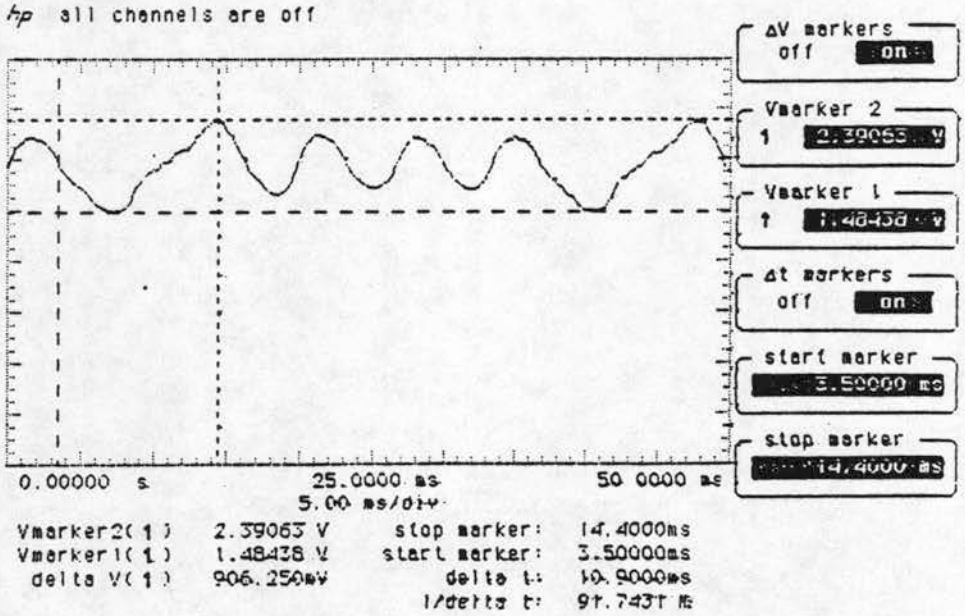

Figure 4.5

Intake Port Pressure at 3200 RPM and Wide Open Throttle

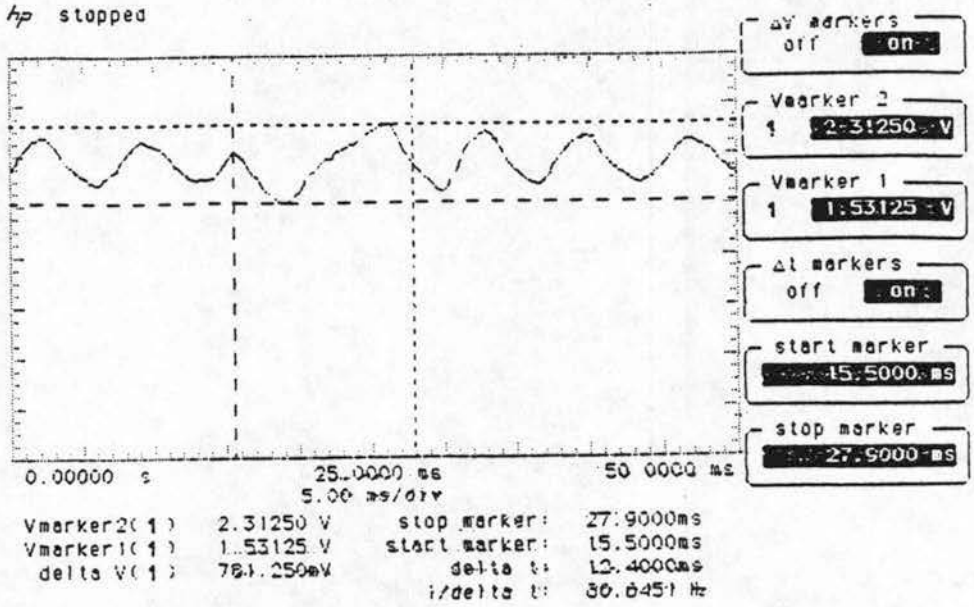

Figure 4.6

Intake Port Pressure at 2800 RPM and Wide Open Throttle

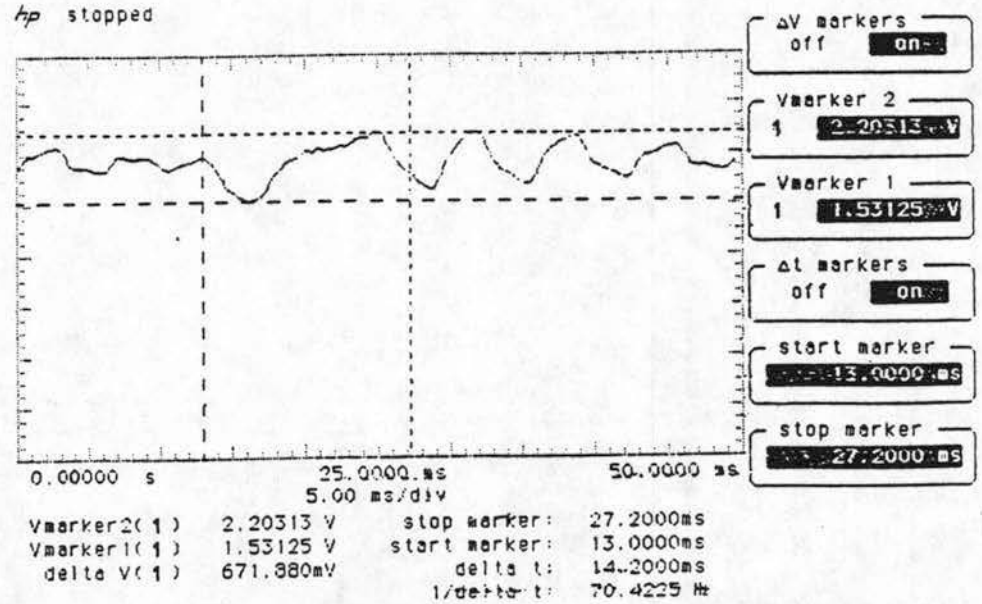

Figure 4.7

Intake Port Pressure at 2400 RPM Wide Open Throttle

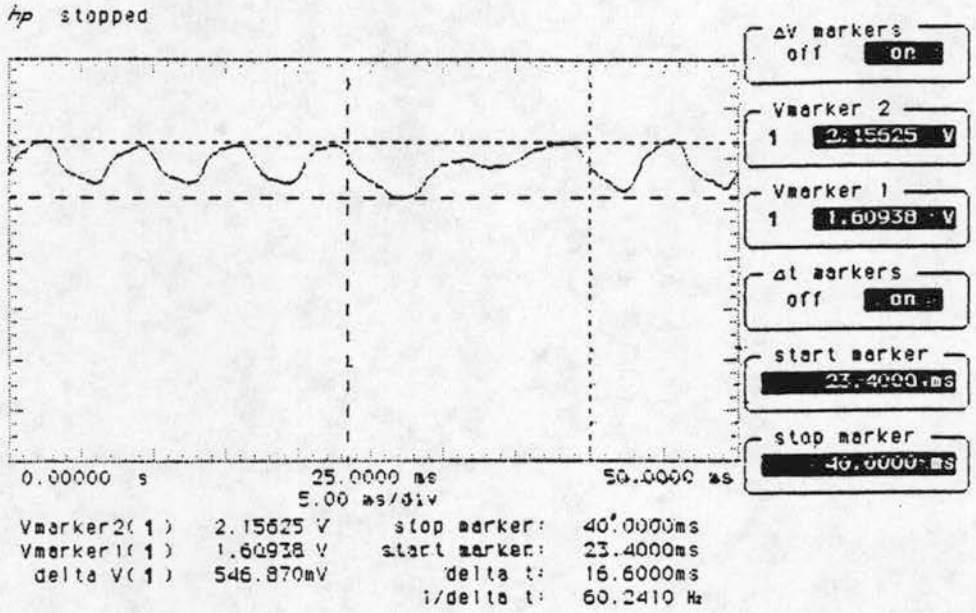

Figure 4.8

The maximum intake pressure reached can be seen in figure 4.9 to increase with increasing RPM, indicating the increased potential for tuning at higher engine speeds. This increase in peak pressure can be attributed to the increase in intake air velocity resulting from the increase in piston speed.

4.2 Throttle Plate Effects on Resonance

During mapping of the fuel injection system, it was observed that the torque produced and fuel required increased significantly with increasing throttle angle near WOT conditions. The sensitivity of torque to throttle changes is expected to decrease as throttle opening increases for a single throttle plate nearing wide open conditions [5]. In order to

further investigate the cause of this effect, torque and intake manifold pressure were measured as a function of throttle angle at a constant 3600 RPM.

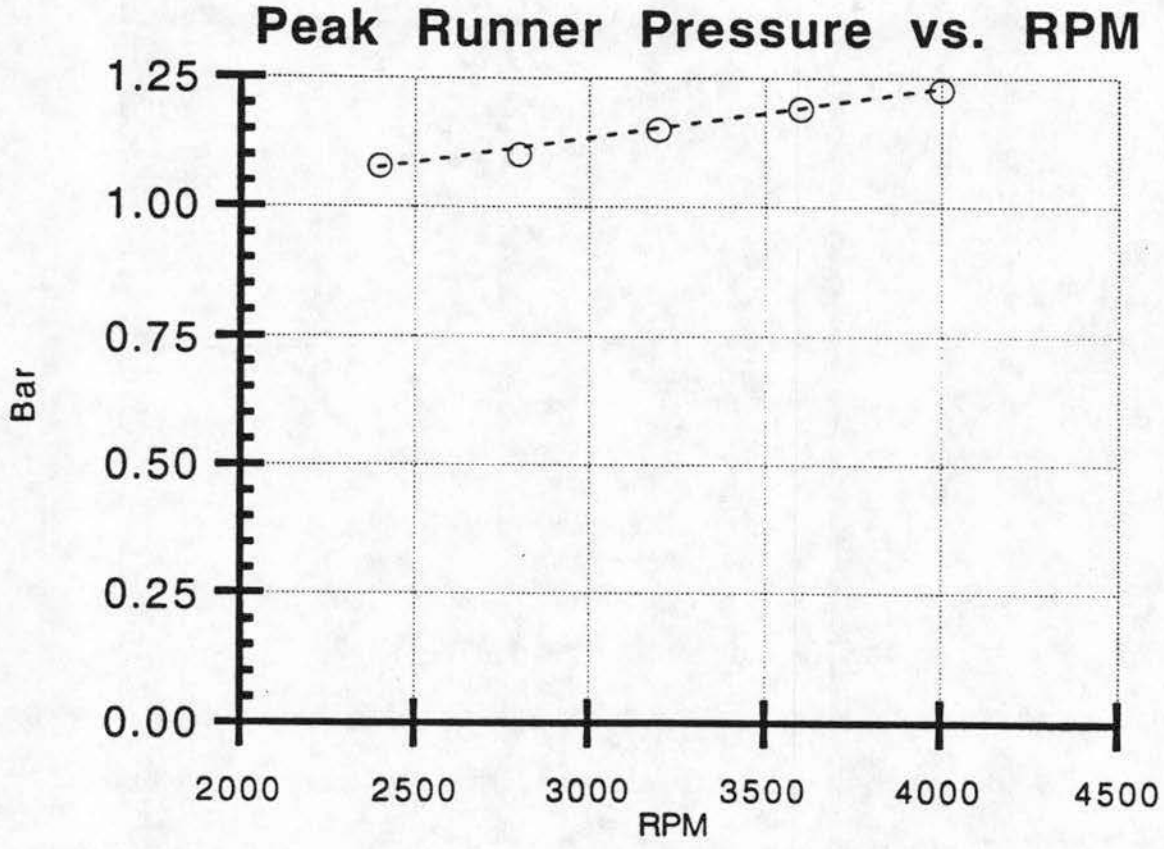

Figure 4.9

Throttle open area perpendicular to the intake runner tubing, calculated from throttle angle[4], was used as an estimate of throttling effect. The percentage of maximum manifold pressure and percentage of maximum torque are plotted against percentage of maximum throttle open area in figure 4.10. Although intake manifold pressure stops increasing when the throttle opening reaches 40% of the maximum area, torque continues to increase significantly up to WOT.

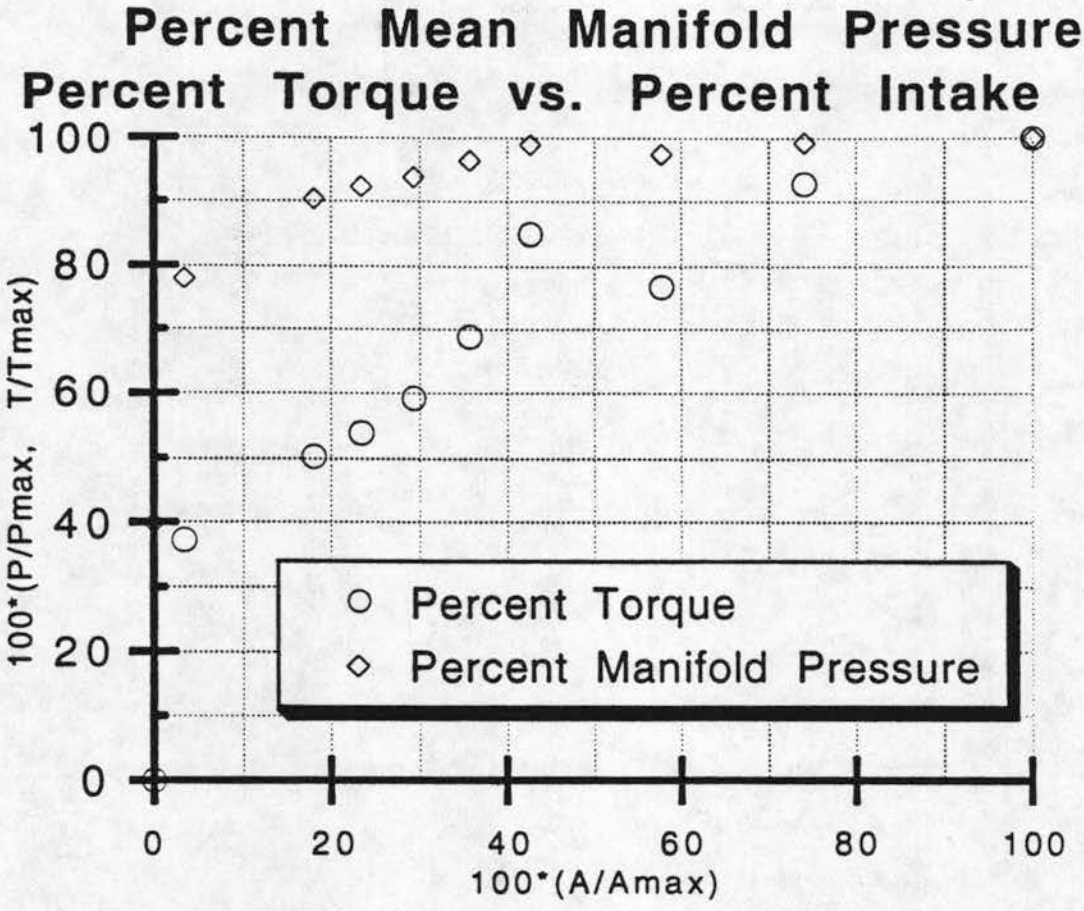

Figure 4.10

In order to better understand the increase in torque at near constant manifold pressure, torque was plotted against manifold pressure in figure 4.11. Torque increase becomes increasingly more sensitive to mean manifold pressure increase as mean manifold pressure increases. For comparison purposes, a simulation of airflow rate vs. intake manifold pressure for a 4700 cc eight cylinder engine with a two barrel carburetor is taken from Heywood [5] and shown in figure 4.12. For intake manifold pressures above 25% of atmospheric, airflow is essentially linear with intake manifold pressure. If the assumption is

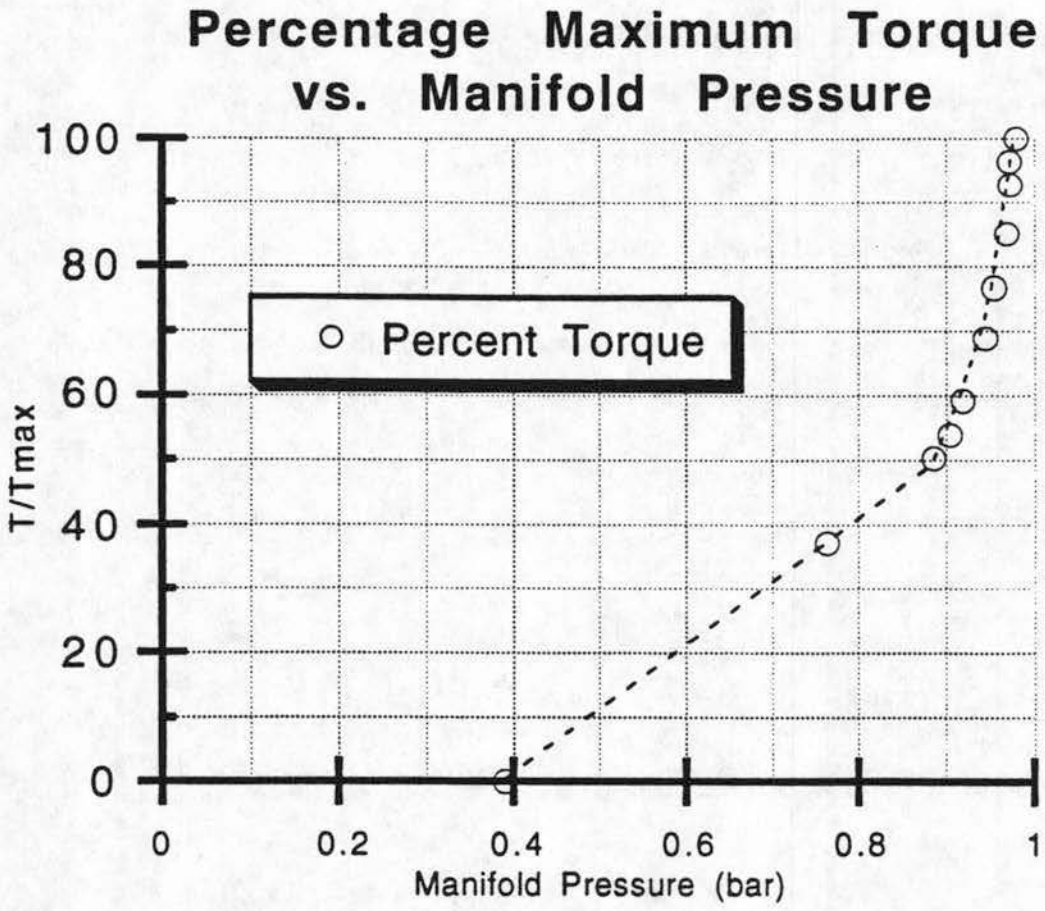

Figure 4.11

accepted that torque is approximately proportional to airflow, then torque for the eight cylinder engine is essentially proportional to manifold pressure. This contrasts significantly with the data for the tuned manifold and. supports the hypothesis that the throttle plates interfere significantly with the resonance effect.

In order to further understand sensitivity of torque to throttle position, intake runner pressure was measured versus time while varying throttle angle at a constant 3600 RPM, see Figs 4.13 through 4.20. The vertical markers indicate intake valve opening and intake valve closing and each large vertical division is .25 bar.

Air Flow Rate Past a Throttle vs. Intake Manifold Pressure with Throttle Angle and Engine Speed

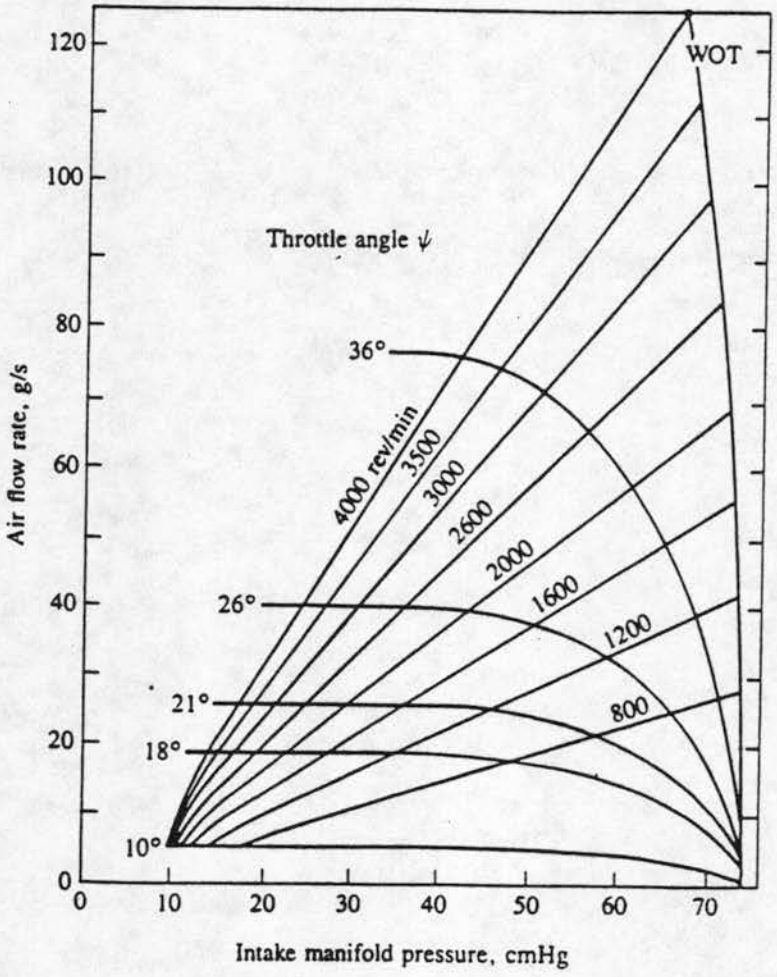

Figure 4.12

Intake Runner Pressure at 3600 RPM

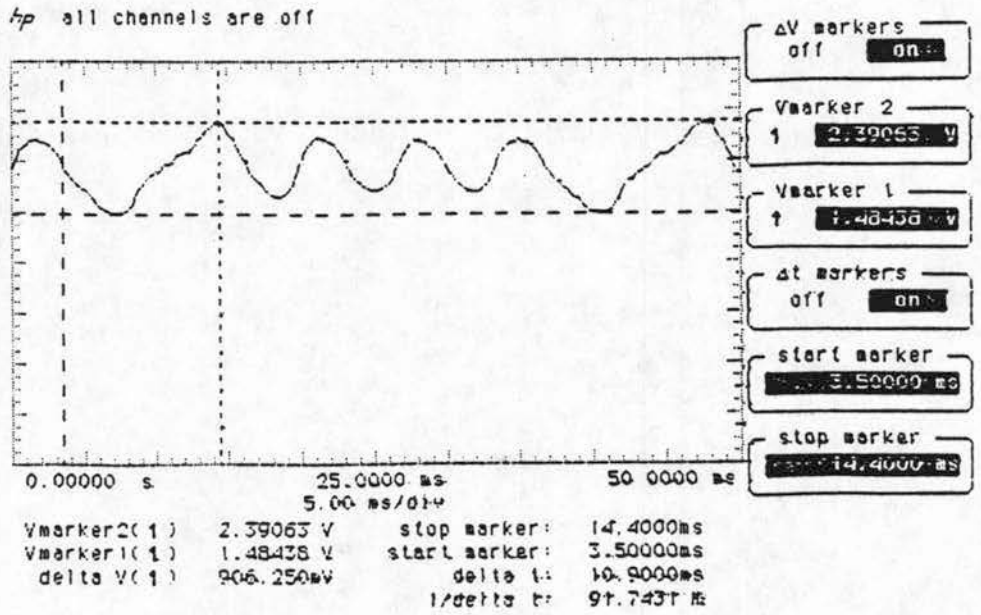

Figure 4.13
100 Percent of Maximum Torque

Intake Runner Pressure at 3600 RPM

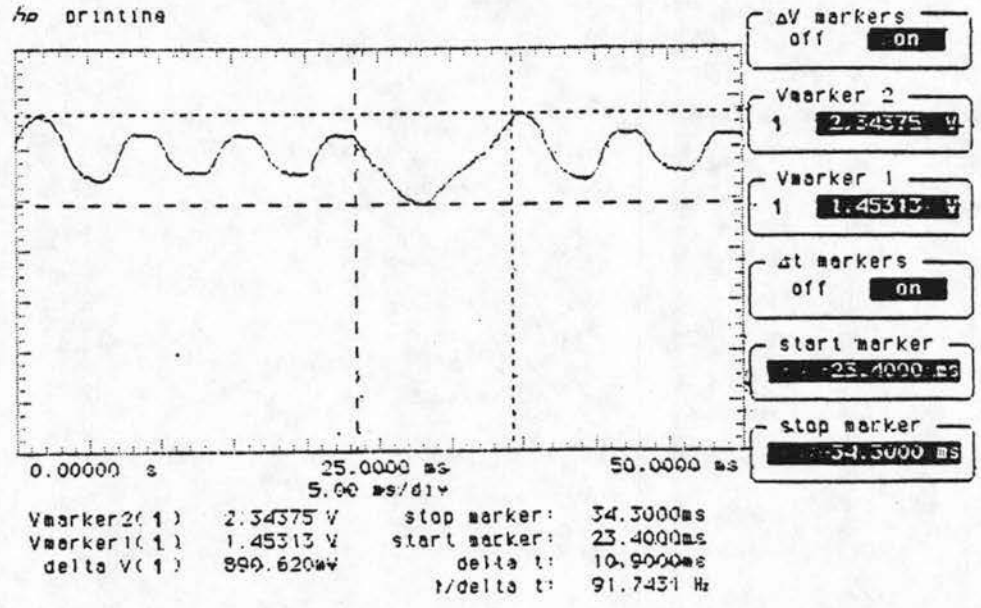

Figure 4.14
92.8 Percent Maximum Torque

Intake Runner Pressure at 3600 RPM

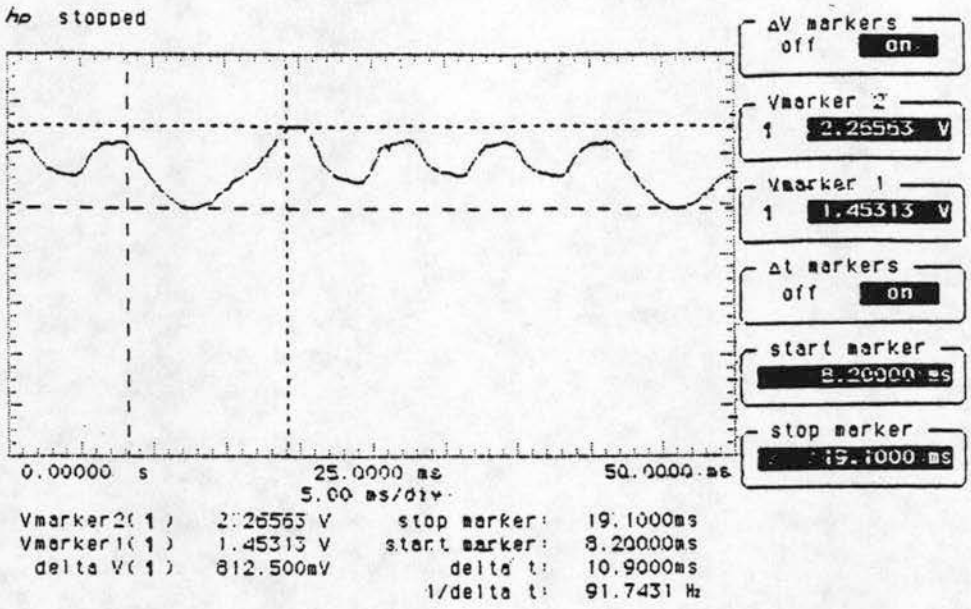

Figure 4.15
85.0 Percent Maximum Torque

Intake Runner Pressure at 3600 RPM

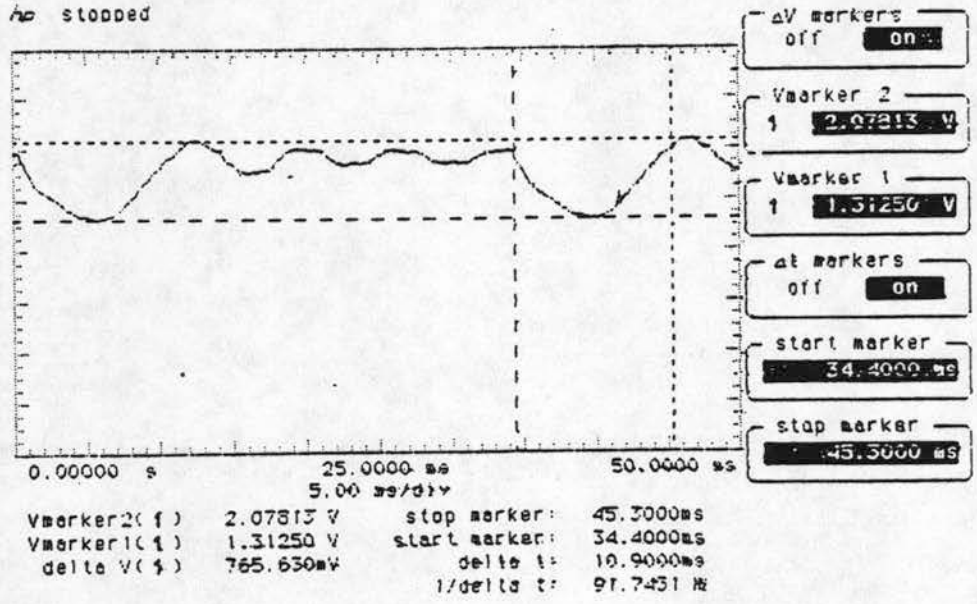

Figure 4.16
68.9 Percent Maximum Torque

Intake Runner Pressure at 3600 RPM

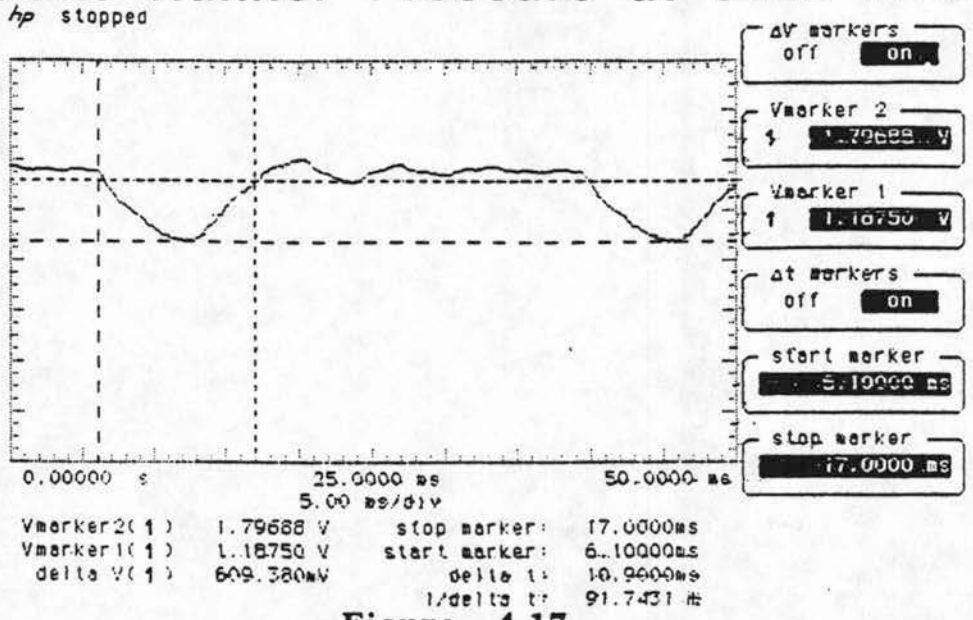

Figure 4.17

59.3 Percent Maximum Torque

Intake Runner Pressure at 3600 RPM

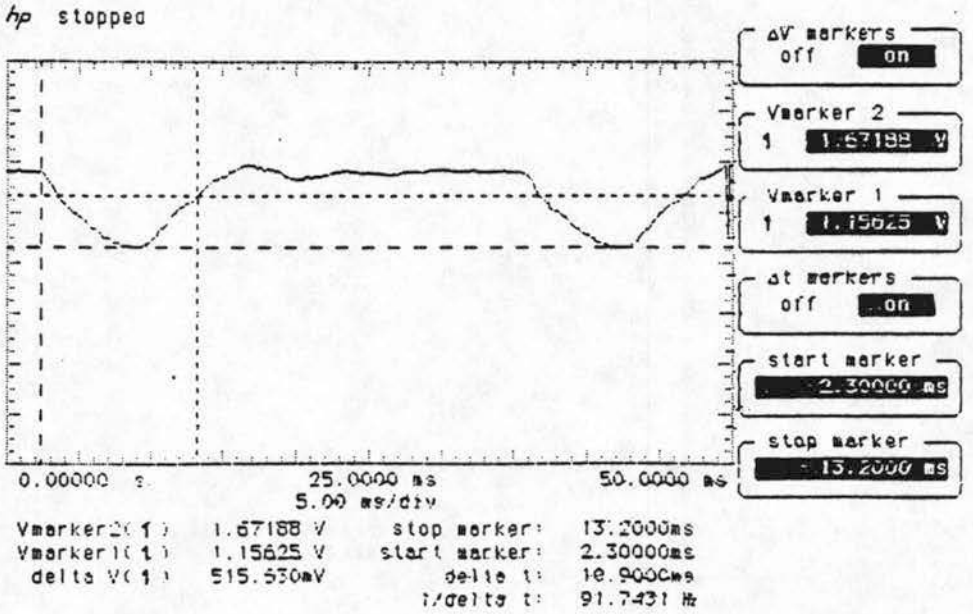

Figure 4.18

53.9 Percent Maximum Torque

Intake Runner Pressure at 3600 RPM

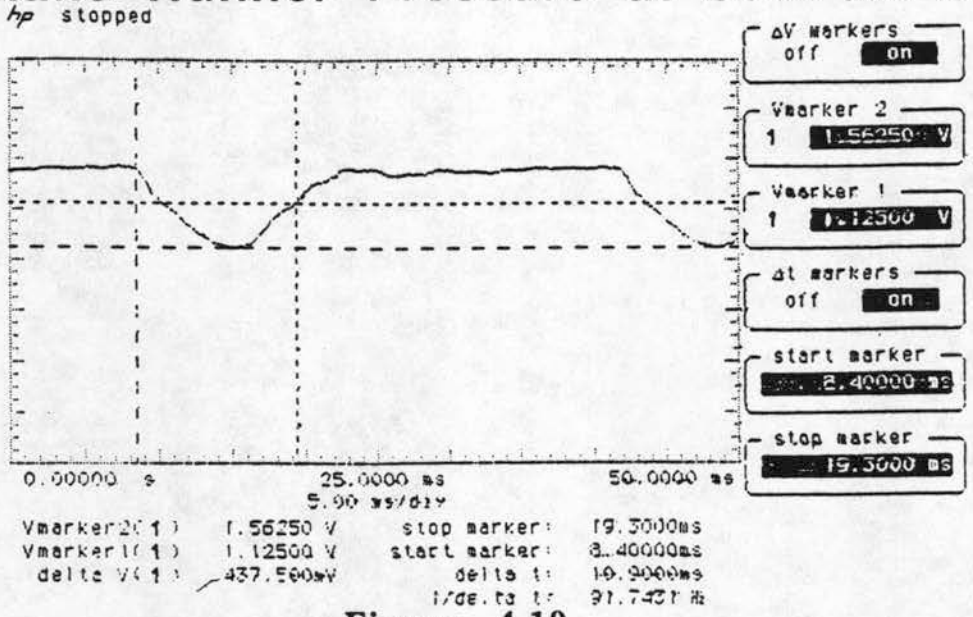

Figure 4.19

50.3 Percent Maximum Torque

Intake Runner Pressure at 3600 RPM

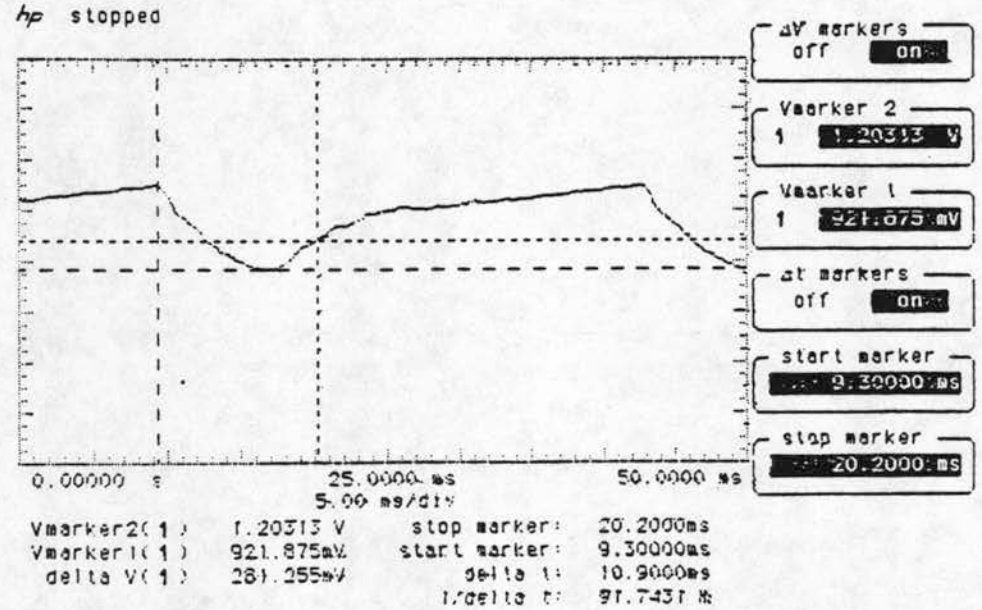

Figure 4.20

37 Percent Maximum Torque

The amplitude of the intake pressure wave is plotted against percentage throttle open area in figure 4.20. Even when mean manifold pressure is relatively constant above 40 percent throttle open area, see figure 4.10, the amplitude of the pressure wave increases with increasing throttle opening, presumably due to the throttle plate interference with the pressure waves.

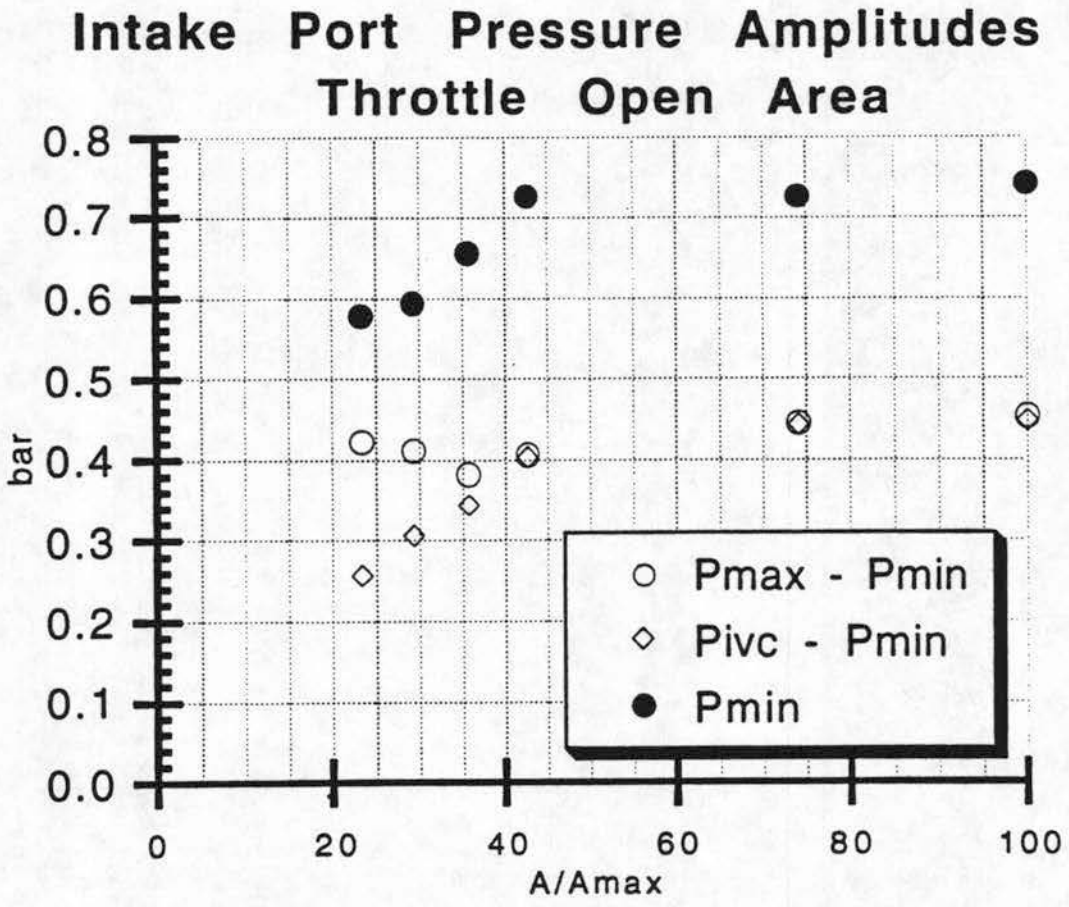

Figure 4.20

Below approximately 40 percent throttle, the pressure wave amplitude begins increasing with decreasing throttle open area, opposite from the trend established at larger throttle openings. This increase in amplitude

can be seen to be due to the reduction in minimum pressure as seen in the minimum intake stroke pressure also plotted on figure 4.20. The reduction in minimum pressure is due to the throttle plate choking during the inrush of the large volume of air during the intake stroke. The difference between pressure at IVC and minimum pressure is also plotted in figure 4.20. This difference can be seen to converge with the amplitude data for large throttle openings. Figures 4.15 through 4.19 show that the reduction in positive pressure at IVC is due to the throttle plate damping the intake stroke and delaying the positive pressure wave until after IVC.

One can make the analogies of the volume of air rushing in during the intake stroke as a mass, the volume in the cylinder as a spring, and the throttle plate as a damper. Accepting these analogies, a throttle open area setting slightly less than 40 percent appears to be the setting for critical damping, with a corresponding phase shift seen in figures 4.12 through 4.19. If it is assumed that the resonance wave centers on the mean manifold pressure, the positive amplitude of the pressure wave divided by the negative amplitude of the pressure wave will give an indication of the magnitude of the damping effect of the throttle plate on the efficiency of the supercharge. Figure 4.21 shows that at WOT, 90 percent of the negative pressure wave amplitude is reflected in a positive pressure wave one half a resonance period later and that nearly 100 percent of it is used to raise the intake port pressure at IVC. That response falls to 70 percent of the negative pressure wave reflected as a positive wave at 43 percent throttle open area, but with the maximum manifold pressure approximately equal to the pressure at IVC. Below approximately 40 percent open area, the positive pressure wave falls to

approximately 30 percent of the negative pressure wave, while the percentage of the negative wave reflected as a positive peak peak at IVC continues to fall and becomes negative. This is because the phase shift due to damping is actually so large that the intake valve closes before the pressure reaches the average value.

The damping of the amplitude of the small pressure waves on the closed intake valve can be seen on the moderately throttled pressure traces, figures 4.17 and 4.18, providing further evidence that the throttle plates interfere significantly with resonance waves in the intake runner.

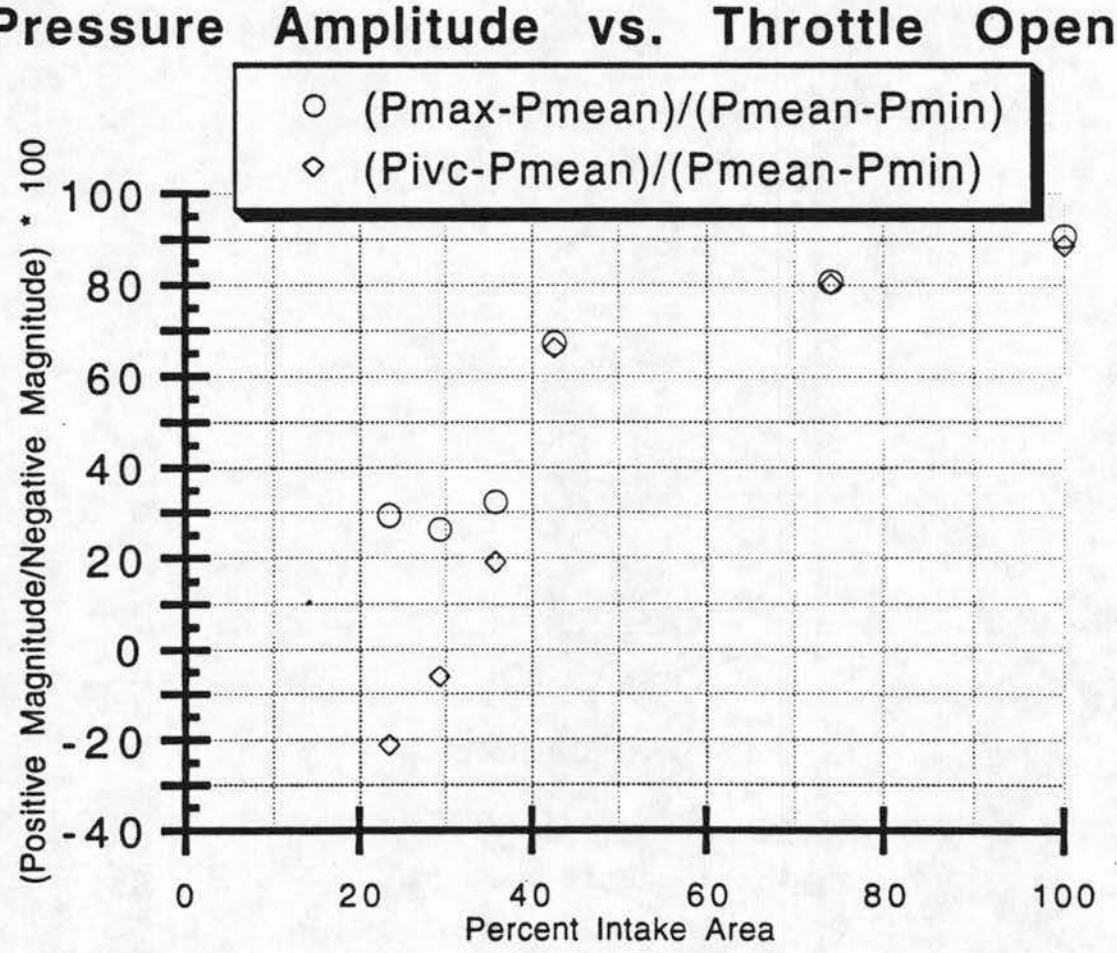

Figure 4.21

Average intake manifold pressure and cylinder port pressure at IVC are plotted against percent maximum torque in figure 4.22 in order to better verify the effect of manifold resonance and the correlation between cylinder port pressure at IVC and torque. At 60 percent torque, average manifold pressure becomes relatively independent of torque at a value slightly below atmospheric and also crosses the curve of intake port pressure at IVC. Intake port pressure at IVC continues to rise up to maximum torque with a maximum observed port pressure at IVC of 1.19 bar, see figure 4.22, indicating significant tuning effect. For the test engine intake port pressure at IVC seems to be a better predictor of torque than average manifold pressure. This relationship

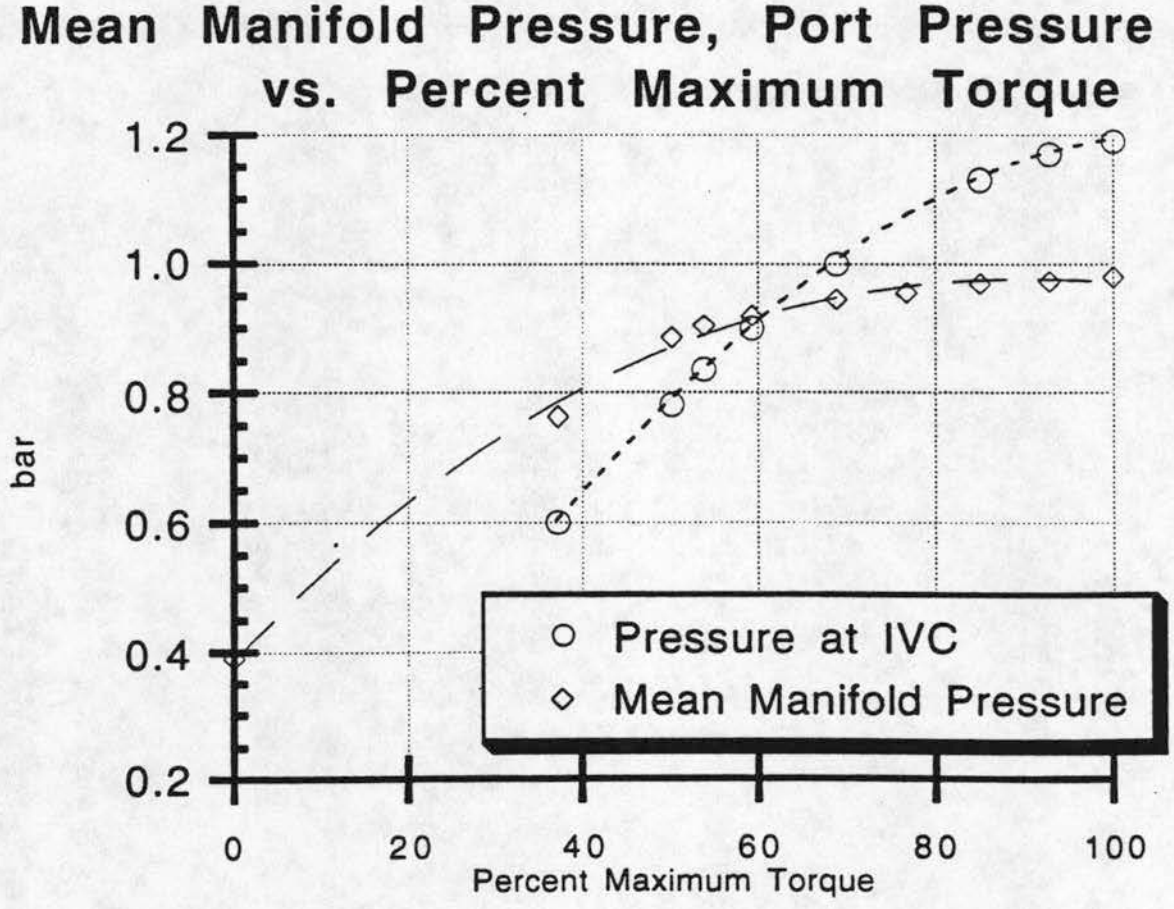

Figure 4.22

validates the use in section 4.1 of manifold pressure at IVC due to resonance as an indicator of the effectiveness of helmholtz tuning.

Based on the preceding data, it appears that the throttle plates in the individual intake runners act as a normal throttle to reduce average intake manifold pressure, but also have a wider range of throttling effect due to their damping of the intake manifold velocity wave during the intake stroke.

5.0 Ethanol Conversion Results and Discussion

In order to convert the throttle body intake system to ethanol operation, the fuel pressure was increased in order to increase the fuel flow rate. When port fuel injectors were used for the new intake system, the fuel injectors were sized for the required higher fuel flow rate at their rated pressure.

5.1 Spark Timing Comparison Between Gasoline and Ethanol

In order to achieve peak efficiency and maximum power while operating with a given fuel, spark timing must be optimized. In order to determine optimum spark advance for gasoline and ethanol, the test engine was run at the design speed of 3600 RPM, stoichiometric air/fuel ratio, and WOT while varying spark advance and measuring torque. Figures 5.1 and 5.2 show the results of varying spark advance Before Top Dead Center (BTDC) on torque output. The torque axis is truncated to better show the effect. From figure 5.1 and 5.2, Maximum Brake Torque (MBT) spark timing at stoichiometric equivalence ratio is 12 degrees BTDC for E95 while gasoline has a knock limit at 16 degrees BTDC. Higher octane gasoline may have a MBT value at a greater spark advance. Since the laminar flame speed of ethanol is slightly lower than that of gasoline [6], the effect cannot be attributed to a shorter ignition delay for ethanol and must be attributed to more a rapid flame speed during the turbulent phase of combustion resulting in a more rapid rise in combustion pressure. This may have beneficial effects on emissions, as discussed in section 6.2. Gasoline spark advance is knock limited in

the test engine as MBT is approached, at WOT and stoichiometric air/fuel ratio using 92 pump octane ((research + motor)/2) unleaded fuel. This is not unexpected, as WOT at a stoichiometric air/fuel ratio is a severe operating condition and the test gasoline has a pump octane rating of 92 compared to E95's pump octane rating of 98 [5].

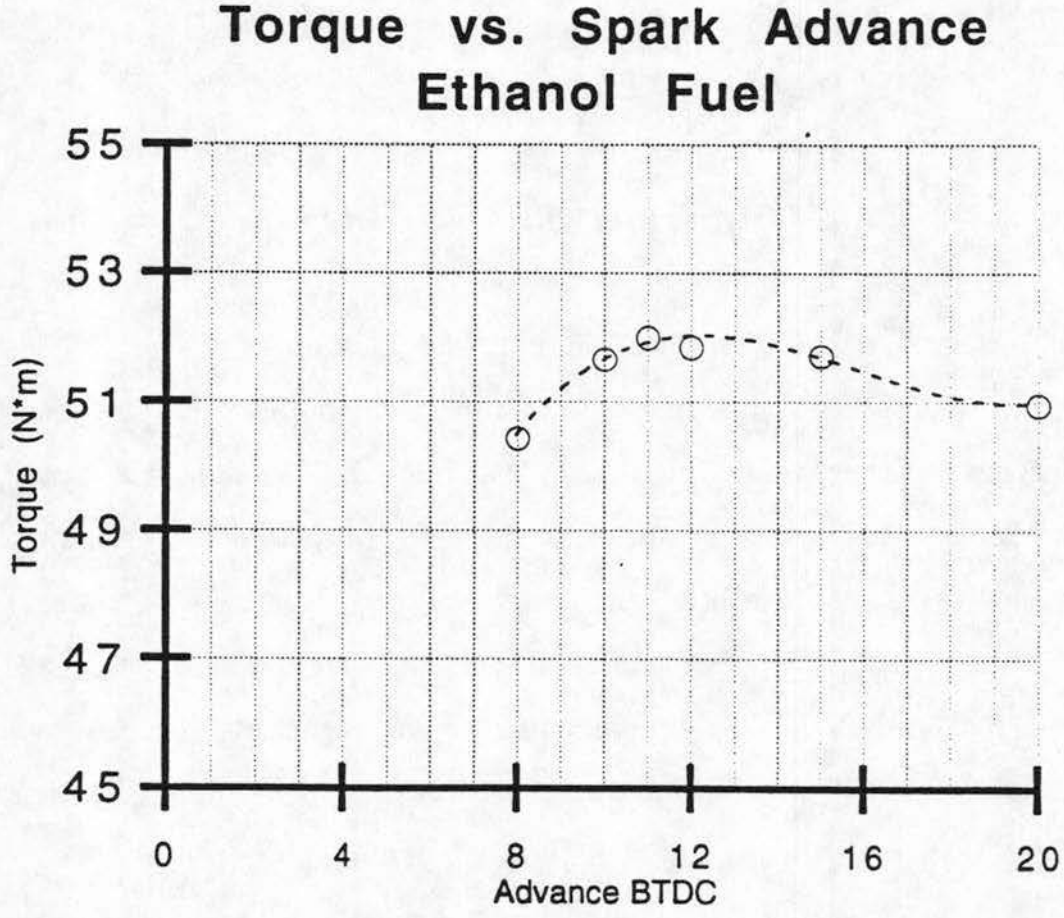

Figure 5.1

Since the engine as supplied by the manufacturer operates at an equivalence ratio of approximately 1.2 and a spark advance of 21 degrees at WOT, the original knock limit may occur at a greater spark advance due to the richer equivalence ratio and due to lower peak pressures resulting from the reduced cylinder filling efficiency of the

original intake manifold. The severe operating conditions of the modified test engine are required, however, for high power levels and effective catalyst action while operating on gasoline, as discussed in section 6.1.

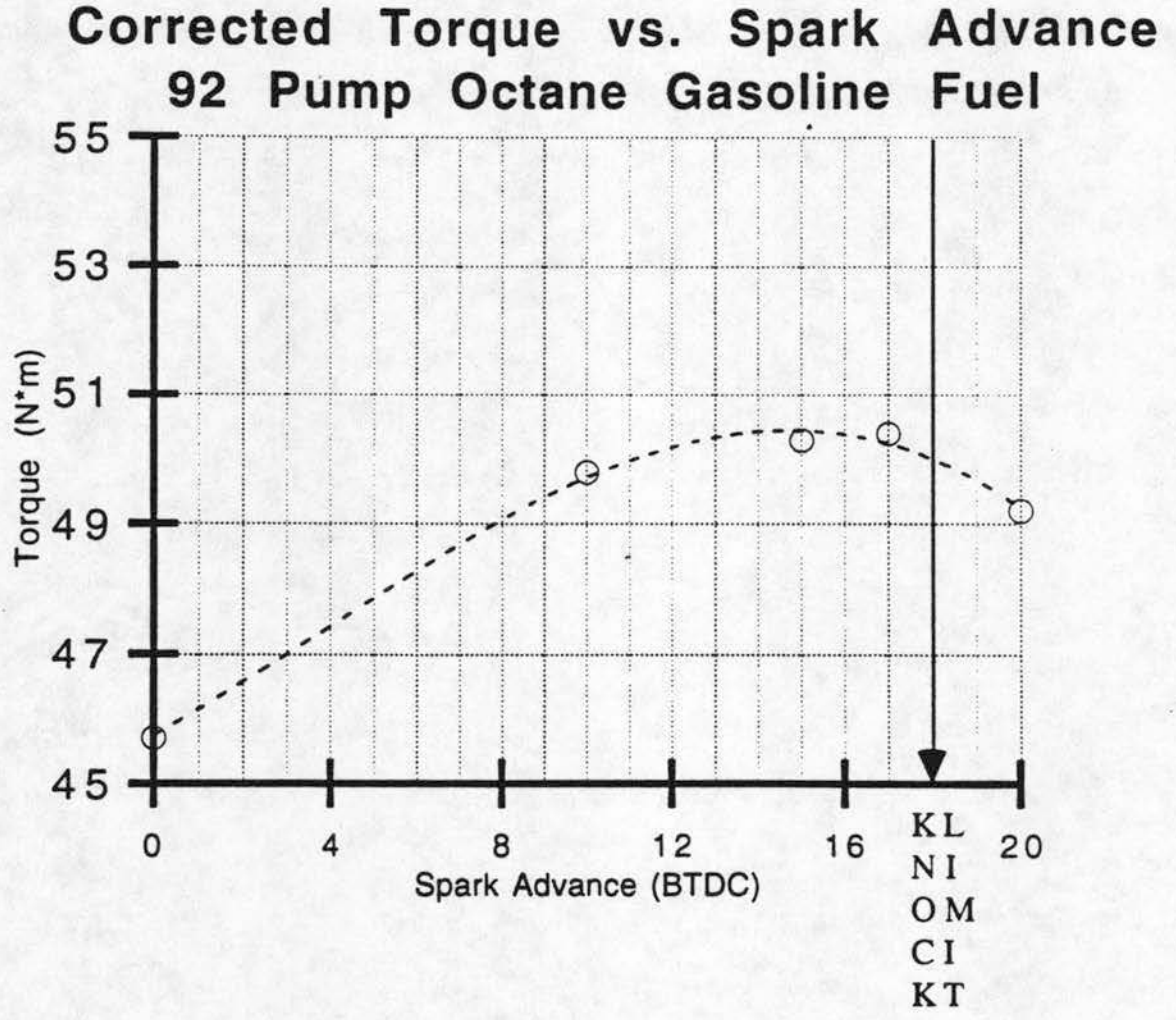

Figure 5.2

5.2 Thermal Efficiency Comparison of Gasoline and Ethanol

Brake specific fuel consumption varies with equivalence ratio at WOT conditions with fixed spark advance. Because the equivalence ratio was calculated from exhaust port emissions which were measured independently for the two cylinders, an average equivalence ratio for the engine is calculated by averaging the equivalence ratio of the two cylinders while assuming constant airflow volume to the two cylinders. In fig 5.3, WOT BSFC at 3600 rpm for both ethanol and gasoline is plotted against the average equivalence ratio of the engine. Although WOT operation allows both power output and BSFC to vary with equivalence ratio, WOT represents the design condition for HEV operation and is therefore the best test condition for this application. BSFC of ethanol was measured at spark advance settings of 10 degrees BTDC which was the MBT spark advance when the tests were uncorrected for atmospheric conditions, and at the manufacturer's nominal advance of 21 degrees BTDC. Increased spark advance can be seen to increase torque and reduce BSFC when running at lean equivalence ratios. Gasoline BSFC was measured at 10 degrees advance to provide a direct comparison with ethanol, although BSFC was also measured with gasoline knock limit timing of 17 degrees. Gasoline BSFC was measured over a narrower range of equivalence ratios because the engine began to misfire and could not maintain the dynamometer speed at 3600 RPM when running at equivalence ratios leaner than .85. The minimum observed BSFC of ethanol was 372 g/Kw*hr and occurred at an equivalence ratio of .8 and a spark advance of 21 degrees. The

minimum observed BSFC of gasoline was 263 g/kw*hr at an equivalence ratio of .92 and a spark advance of 17 degrees.

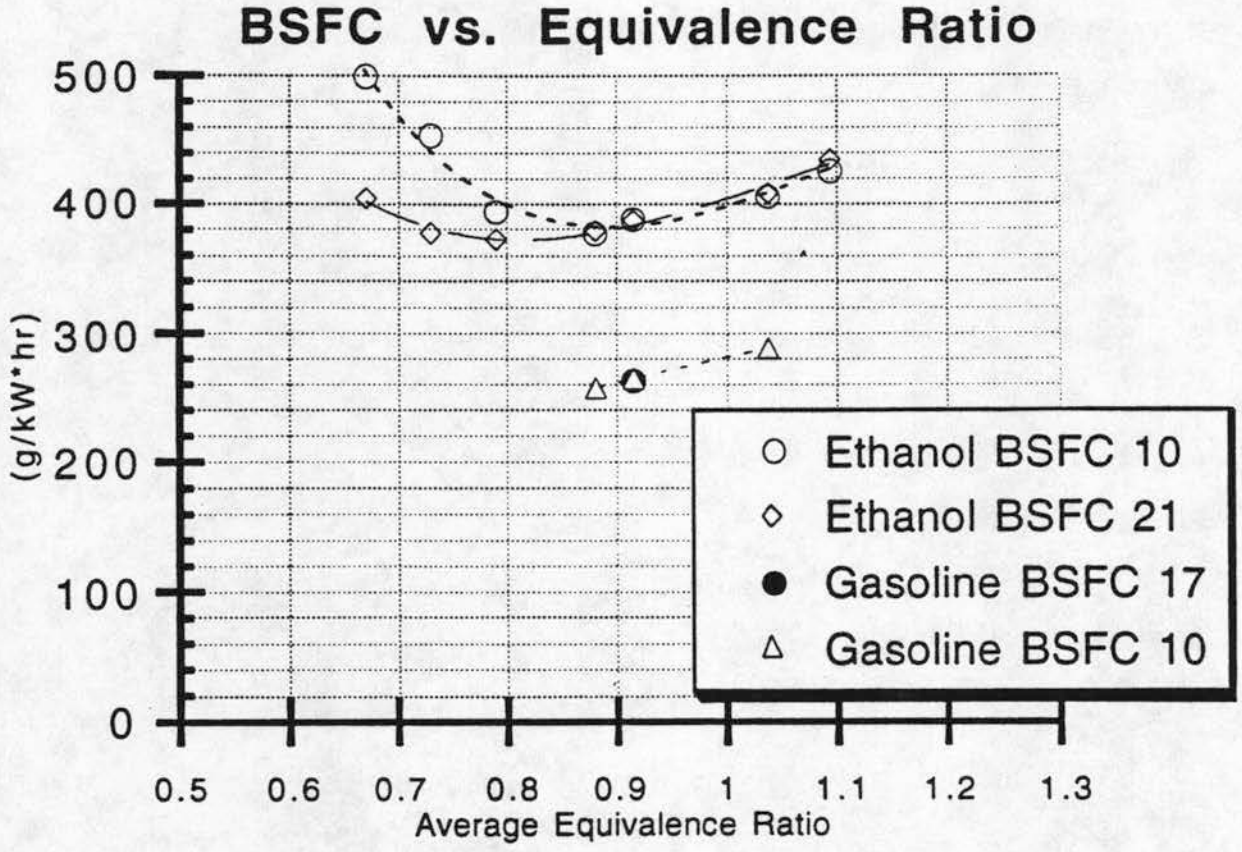

Figure 5.3

Thermal efficiency was calculated from BSFC and the heating value of the fuel and plotted in figure 5.4 in order to get a non-dimensional comparison between ethanol and gasoline. At an equivalence ratio of .91, the calculated thermal efficiency was 33.5% for ethanol based on a lower heating value of 27.8 MJ/kg for a 95% ethanol/5% gasoline blend and 31.1% for gasoline based on a lower heating value of 44.0 MJ/kg [5]. The thermal efficiency while operating with ethanol rose to 34.9% at an

equivalence ratio of .79 with a spark advance of 21 degrees BTDC. The higher thermal efficiency achievable when operating with ethanol relative to gasoline is the result of the combination of a higher thermal efficiency during stoichiometric WOT operation and a further increase due to the ability to run at lean equivalence ratios without severe misfire where higher thermal efficiency is achievable.

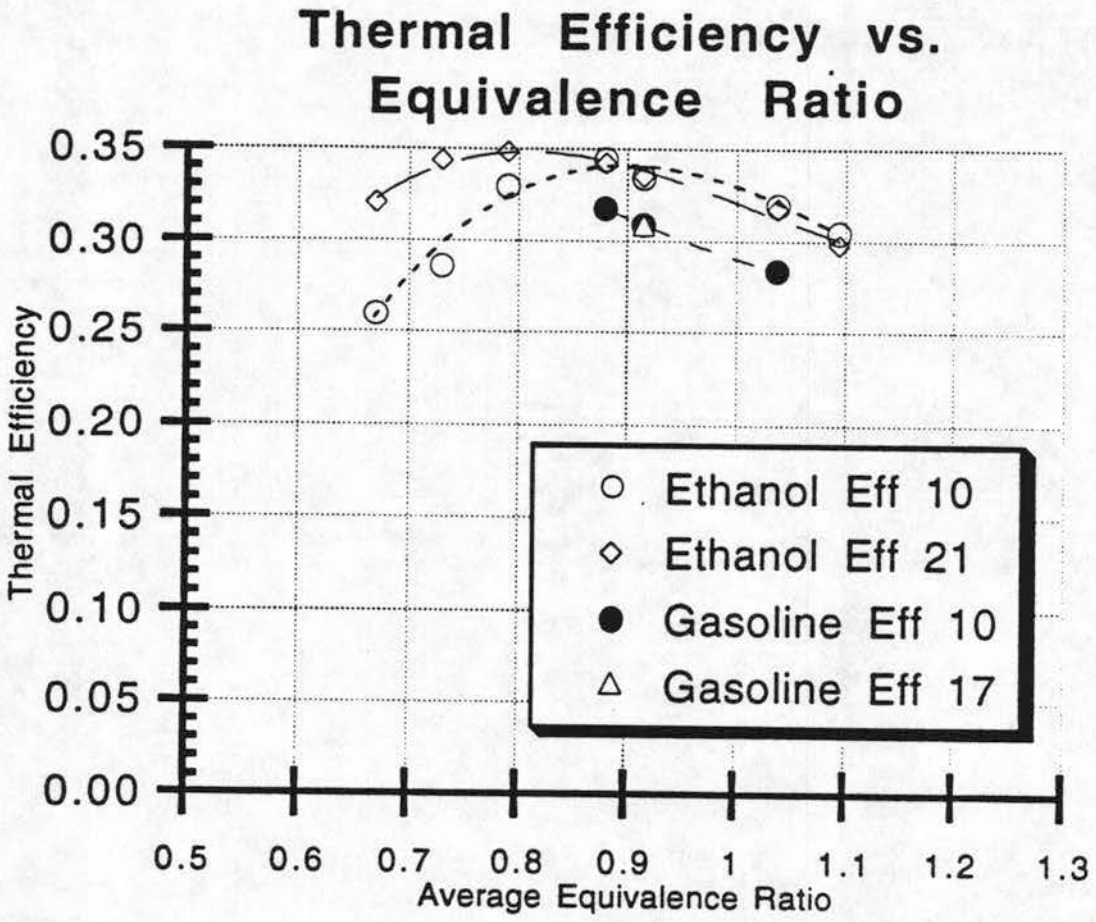

Figure 5.4

Operation at lean air fuel ratios results in some loss in maximum power output. WOT Torque is plotted versus equivalence ratio in figure 5.5 at different spark advance settings. Operating at an equivalence

ratio of .8 instead of 1.0 results in a decrease in torque output of 8% from 52 N*m to 48 N*m, however fuel consumption falls from 400 g/kw*hr to 372 g/Kw*hr, a decrease of 9.5%.

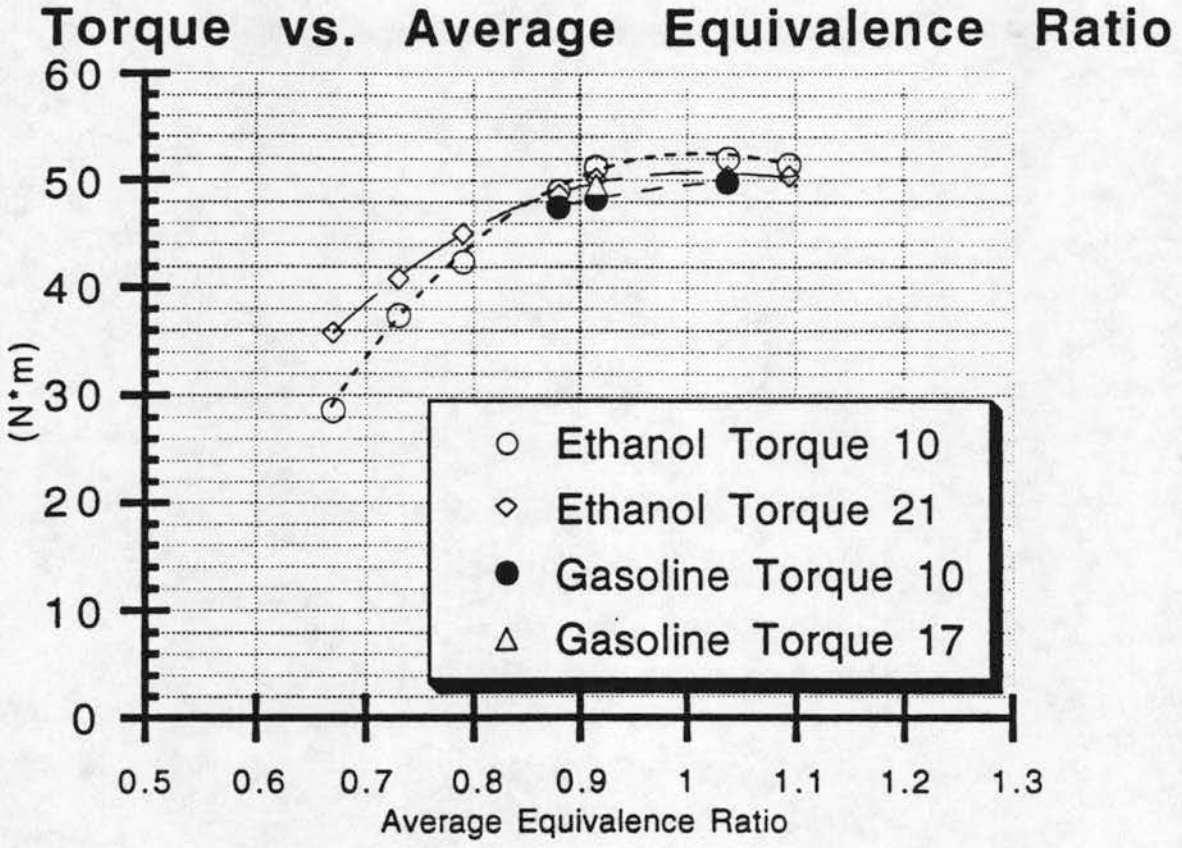

Figure 5.5

6.0 Emissions Results

The uncatalyzed emissions of the engine were measured directly at the exhaust port of each cylinder. The basic exhaust gas composition of the engine consists of CO_2, CO, and O_2, with small percentages of HC and NOx.

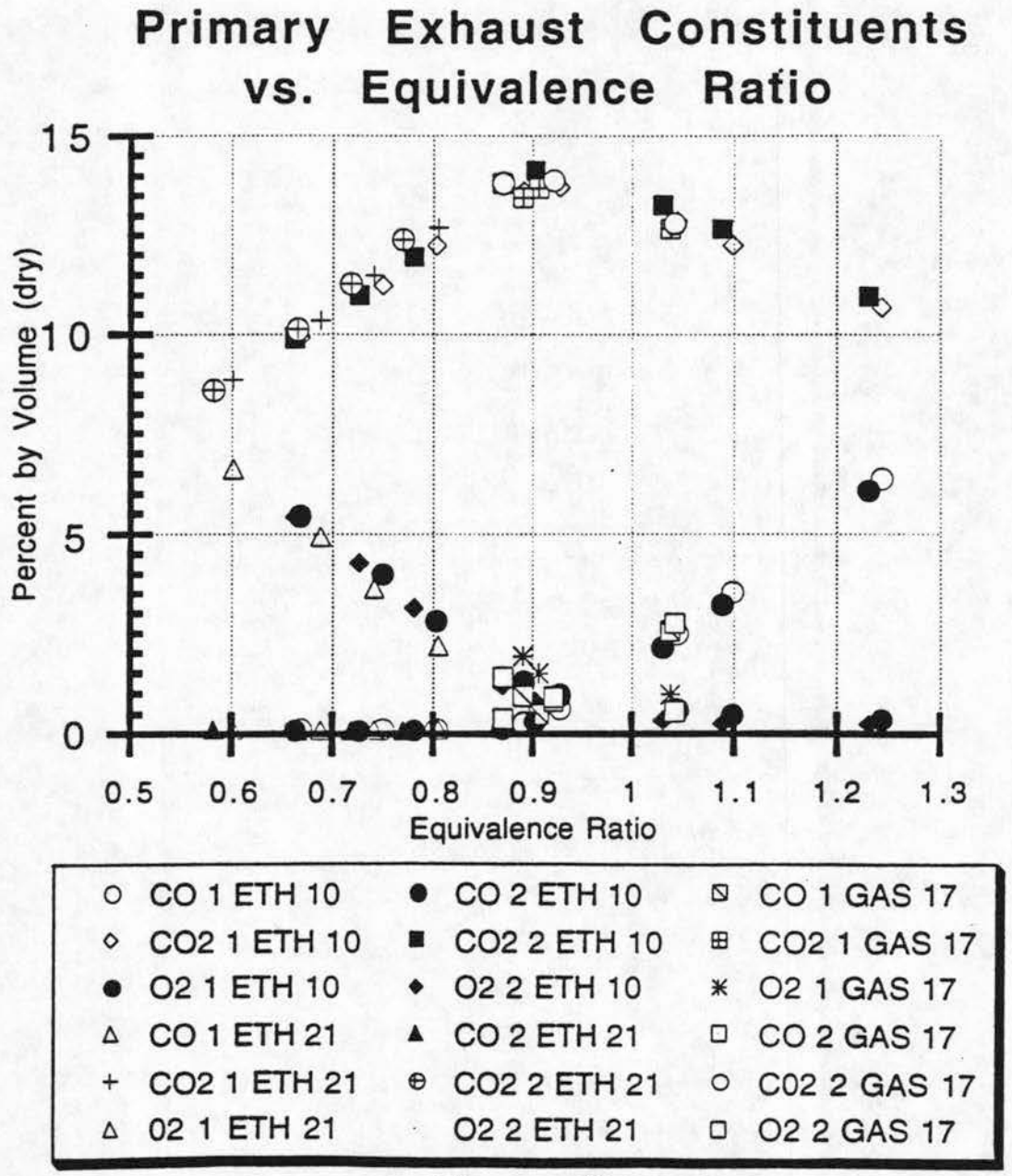

Figure 6.1

6.1 Primary Emissions

The primary exhaust components CO_2, CO, and O_2 are plotted vs. equivalence ratio at WOT in figure 6.1 with different indicators for both gasoline and ethanol, for both cylinders, and all spark advance values. The emissions of these components appear to be essentially independent of fuel type, cylinder, and spark advance. The data follow expected trends and correlate almost exactly with the data published in Heywood [5] and shown in figure 6.2.

Primary Exhaust Constituents vs. Equivalence Ratio

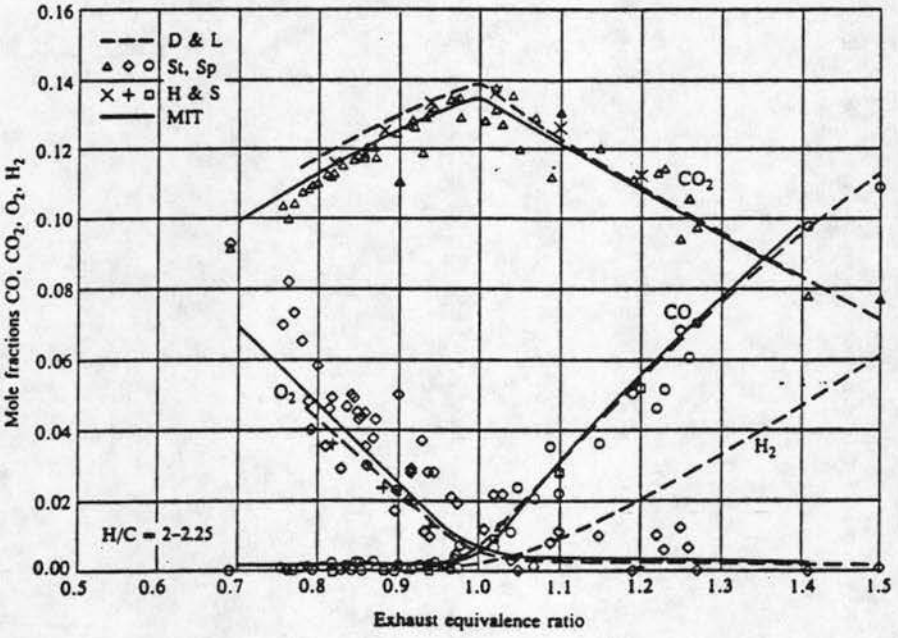

Figure 6.2

Since HEV architecture allows engine operation independent of vehicle demands, viewing emissions in a brake specific format provides a better understanding of the compromises involved in minimizing emissions. BSFC values and air/fuel ratio were used to convert from

percentages to units of g/Kw*hr. This is a better primary measure of emissions for series hybrid operation. From the results plotted in figure 6.3, it can be seen that CO emissions are minimized by operating at lean equivalence ratios. While operating with ethanol fuel at the two equivalence ratios where thermal efficiency is maximized for a given spark advance, CO_2 emissions were approximately equal at 58000 g/kw*hr. Due to the fixed carbon content of the fuel, if CO and HC emissions are small and consequently ignored, specific CO_2 emissions are solely a function of specific fuel consumption as effected by optimization of spark advance and equivalence ratio. Specific CO_2 emissions while

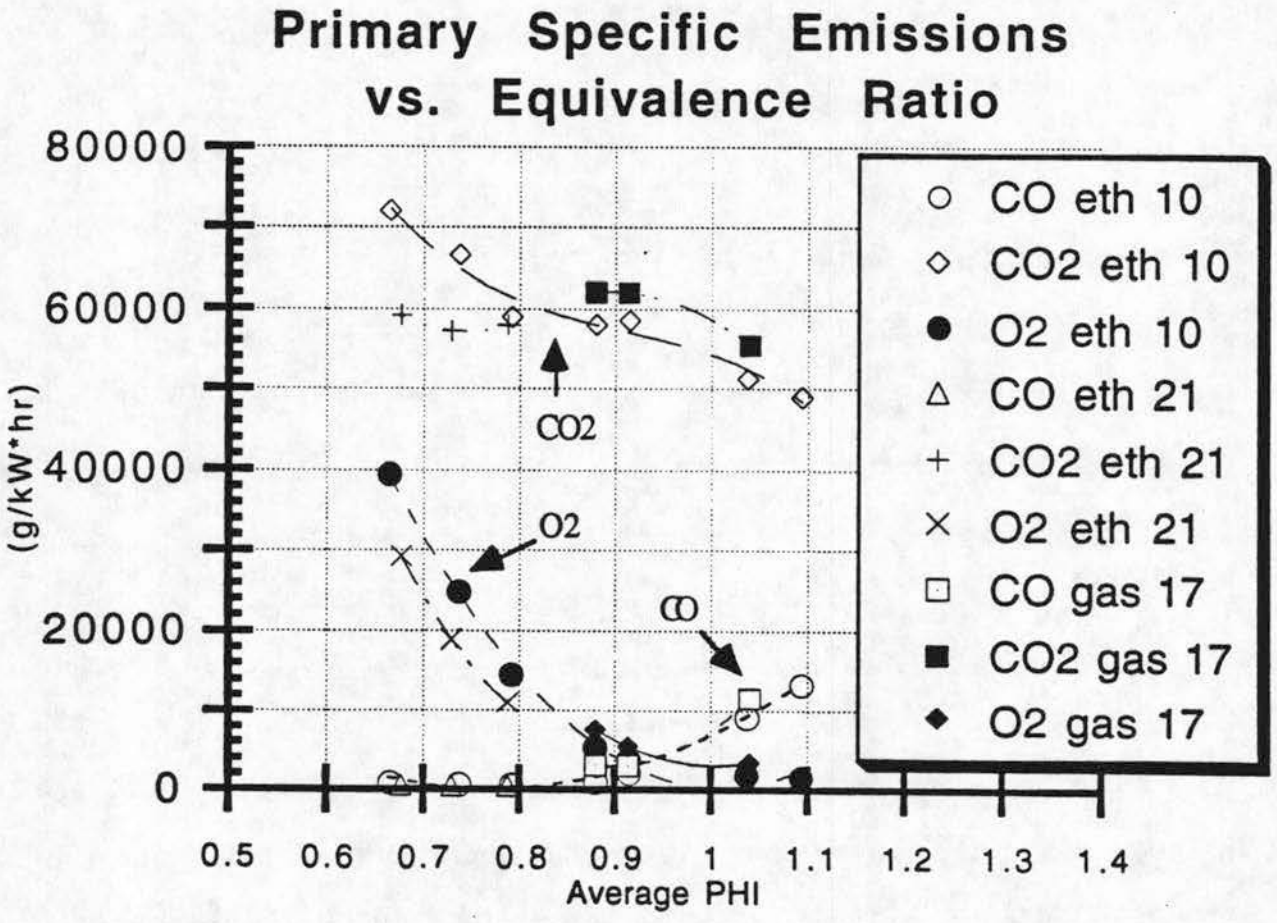

Figure 6.3

operating on gasoline are slightly higher at 62000 g/kw*hr due to the lower thermal efficiency of gasoline. Oxygen emissions are not a pollutant and do not need to be minimized.

6.2 HC and NOx Emissions

Modern three way catalytic converters are capable of reducing both HC and CO emissions via an oxidation reaction and NOx emissions via a reduction reaction. High efficiency for both reactions is restricted to a narrow range of equivalence ratio around stoichiometric with lean air/fuel ratios resulting in low NOx reduction conversion efficiency and rich air/fuel ratios result in low HC and CO oxidation efficiency. For an aged catalyst, the conversion efficiencies of HC and NOx are about 90% at an equivalence ratio of 1.001 [5]. Peak efficiency of a three way catalyst is restricted to equivalence ratios of .999 to 1.007 for a window of 80% efficiency[5]. This operational range can be broadened to about .06 equivalence ratio units by cycling the fuel flow at .5 to 1 hertz [5].

Unfortunately the equivalence ratio for optimal catalyst efficiency does not correspond with the equivalence ratio for minimum BSFC and also results in high pre-catalyst NOx emissions. Due to the lean flammability limit of gasoline, engines cannot operate at sufficiently lean equivalence ratios to lower pre-catalyst NOx emissions. Thus, high pre-catalyst NOx emissions and higher than optimum fuel consumption must be accepted in order to achieve low post catalyst emissions of HC, CO, and NOx.

Part per million emissions of hydrocarbons and oxides of nitrogen were measured at WOT at spark advances of 10 and 21 degrees for ethanol and 17 degrees for gasoline. Emissions were measured from

each cylinder independently. Percentage hydrocarbon emissions are plotted in figure 6.4 against equivalence ratio. Percentage hydrocarbon emissions during ethanol operation can be seen to reach a minimum at an equivalence ratio of approximately .8. Increasing spark advance reduces the hydrocarbon emissions at air fuel ratios leaner than .8 This may be attributed to increased combustion time and efficiency. In the test engine, the hydrocarbon emissions of cylinder number 1 are approximately 50% greater than the emissions for cylinder number 2.

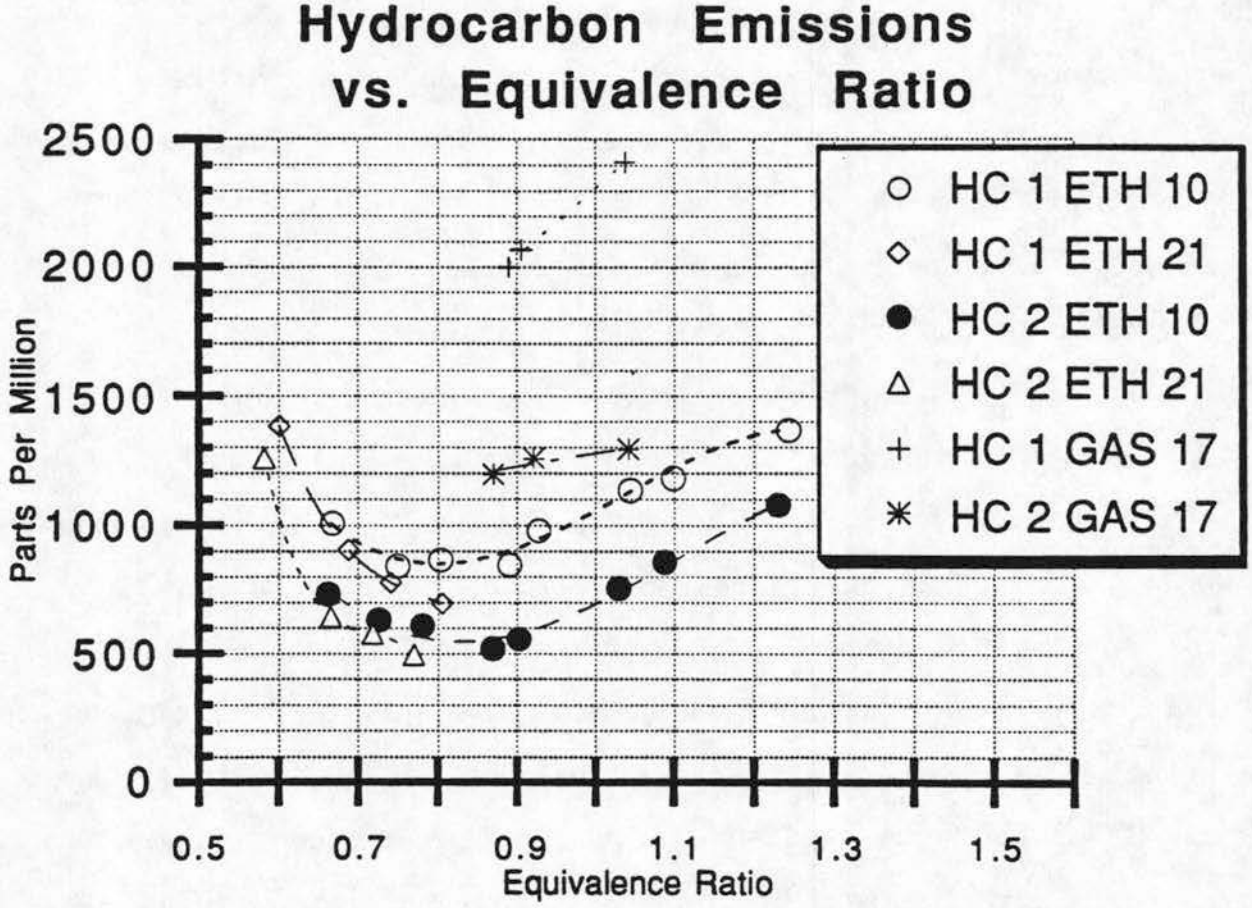

Figure 6.4

The reason for this is not known but may be due to fuel injector placement and fuel vaporization, operating temperature of the cylinder, exhaust valve sealing, or wear condition of the cylinder allowing more

oil to remain in the combustion chamber. Hydrocarbon emissions when using ethanol as a fuel were found to be approximately 50% of the hydrocarbon emissions when using gasoline at the equivalence ratios tested. One possible reason for lower HC emissions is the oxygen content of ethanol promoting more complete combustion. The reduced spark advance required by ethanol relative to gasoline implies more rapid combustion and that the combustion is more complete while the combustion temperatures and pressures are high. .These conditions would promote more complete combustion. More rapid combustion would also reduce NOx emissions if the shorter duration of high temperature and pressure due to reduced spark advance outweighed any increase in peak temperature and pressure.

Percentage emissions of oxides of nitrogen are plotted in figure 6.5. NO_X emissions can be seen to peak at an equivalence ratio of approximately .9 and to increase with increasing spark advance at lean equivalence ratios. Increasing spark advance results in increased peak pressures and temperatures, increasing NOx emissions. Cylinder 2 emissions of NO_X are approximately 20% higher than for cylinder 1. Since equivalence ratio is calculated independently for each cylinder and used as the independent variable for the plot, emissions variations solely due to cylinder to cylinder variations in equivalence ratio should fall on the same curve. Since cylinder 2 can be seen to consistently run at a leaner equivalence ratio than cylinder 1, it may have a higher volumetric efficiency due to variations in port design and intake manifold fabrication. This higher initial cylinder charge would result in higher peak pressures and temperatures. Cylinder 2 also has lower HC emissions than cylinder 1, possibly indicating better sealing of the

cylinder and further promoting higher peak pressures. NO_X emissions are below 1000 ppm at equivalence ratios below approximately .65. Further optimization of spark advance may lower NOx emissions enough so that reduction by catalyst is not required, however MBT spark timing for a given equivalence ratio results in higher pressures and temperatures and therefore higher NO_X emissions. One disadvantage to operation at this point is a reduction of approximately 25% in power output relative to MBT timing at an equivalence ratio of 1.0 as seen fig 5.5.

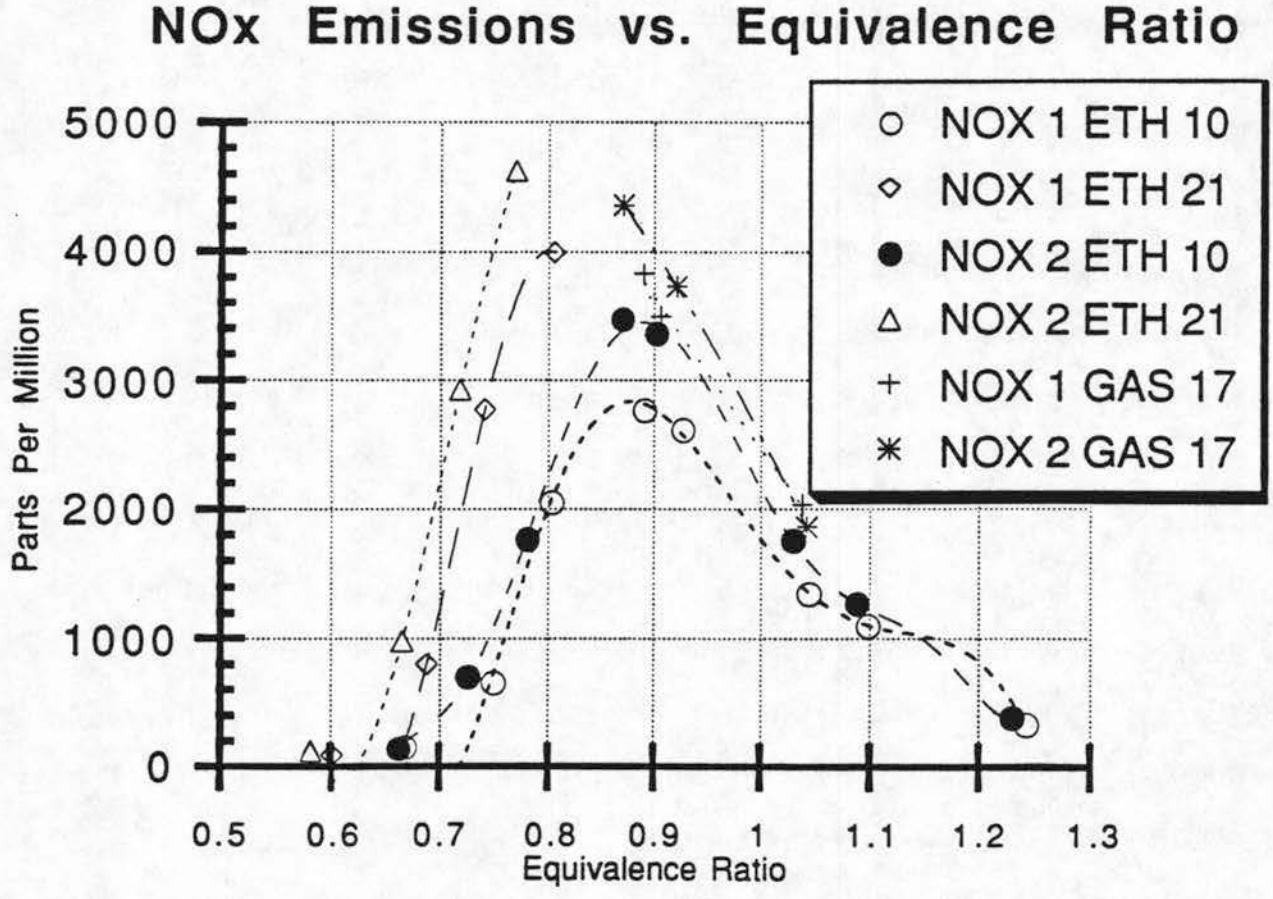

Figure 6.5

In order to give a better measure of emissions for HEV operation, average brake specific emissions for the engine were calculated from BSFC, average air/fuel ratio for the cylinders, and average percentage emissions. Specific emissions of HC and NO_X as a function of equivalence ratio are plotted in figure 6.6. Ethanol can be seen to reduce maximum NO_X emissions by 29% from 19 g/Kw*hr to 13.5 g/kw*hr when operating near stoichiometric. This reduction may be due to the significantly higher heat of vaporization of ethanol relative to gasoline lowering the peak temperature of combustion. The energy required to vaporize the ethanol in a stoichiometric mixture of ethanol and air is 3.89 times the energy required to vaporize the gasoline in a stoichiometric mixture of gasoline and air[5]. This energy results in a temperature drop due to adiabatic vaporization of a stoichiometric charge of 21.4° C for gasoline

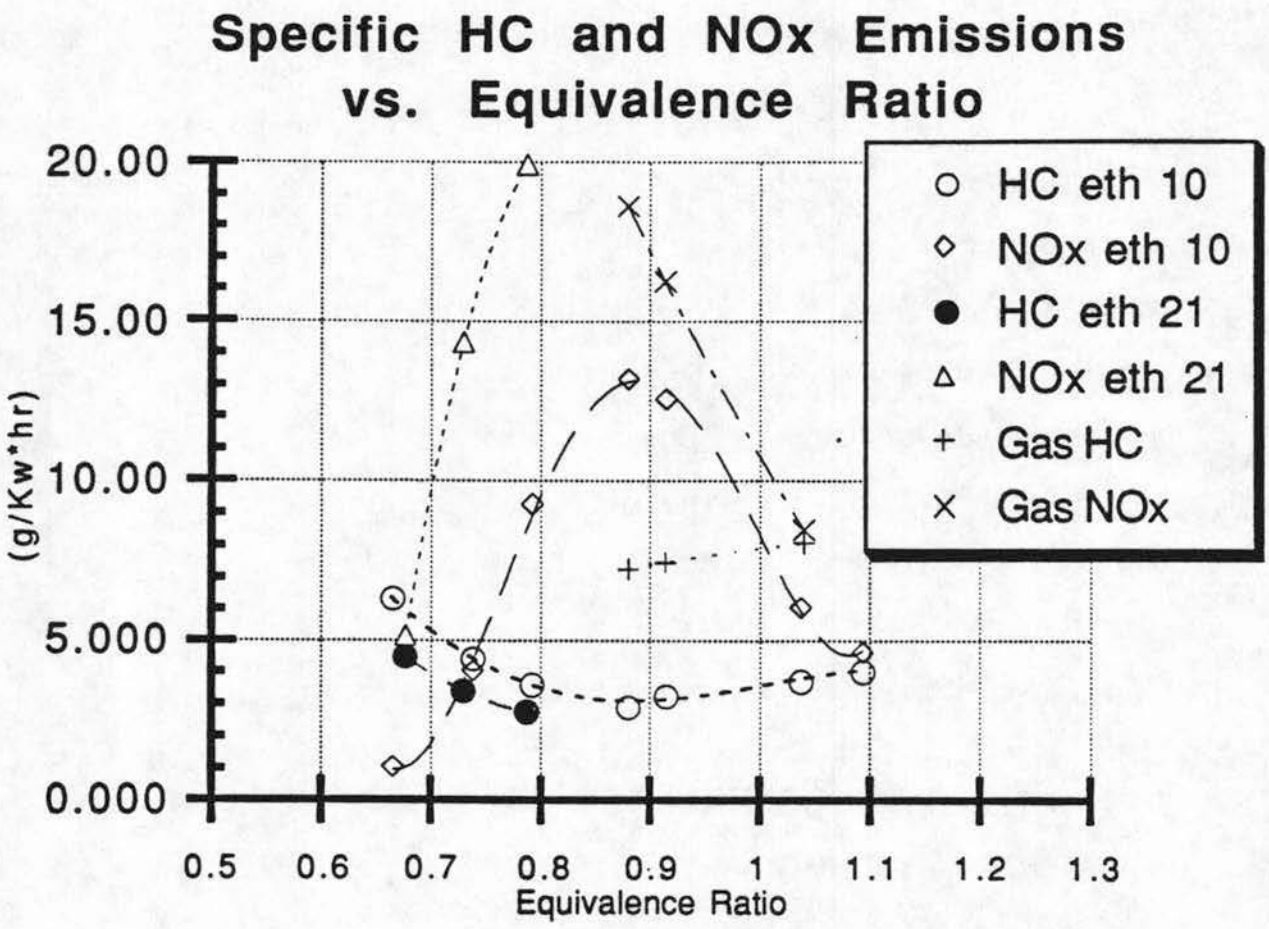

Figure 6.6

and 76.5° C for ethanol. The reduced NOx. emissions may also be due to the more rapid combustion and reduced spark advance which may reduce the time spent at high temperatures and pressures. Specific NO_X emissions have a much higher peak for ethanol when operating at 21 degrees advance, but specific NO_X emissions below that of gasoline can be achieved by operating at equivalence ratios below .7. Specific HC emissions of ethanol are approximately 50% of those for gasoline over the ranges tested, and a minimum of 2.8 g/Kw*hr can be achieved with ethanol vs. a minimum of 7.5 g/kw*hr for gasoline.

An alternative operating point when using ethanol in this application is at an equivalence ratio of approximately .68 to .75 and a spark advance of between 10 and 21 degrees. This region of operation has low BSFC and low uncatalyzed specific NOx and HC emissions. Increasing spark advance from 10 degrees to 21 degrees reduces BSFC and increases torque at the penalty of increased NOx emissions as can be seen in figures 5.3, 5.5, and 6.6. Reducing equivalence ratio results in lower NOx emissions but increased HC emissions and reduced torque as can be seen in figure 5.5. There is an excess of oxygen at this point, allowing easy oxidation of HC emissions if NOx emissions are already significantly lowered. Further testing in this operating region with varying spark advance may provide a better compromise than the spark advance values tested.

7.0 Conclusions

The simple two leg manifold and throttle body fuel injection system supplied by the manufacturer have a number of disadvantages for the test engine. These disadvantages include fuel maldistribution, up to approximately 20%, and a reduction in power relative to a tuned intake manifold.

Helmholtz theory accurately predicted the length of intake runner required for maximum tuning at the design RPM. No further information about intake manifold characteristics was required and the results were obtained with simple calculations. The complete tuned intake system increased torque by 28% over the simple two leg manifold at the design speed. The combination of port fuel injection and the separation of intake runners reduced cylinder to cylinder fuel maldistribution from approximately 20% to a range of 1% near stoichiometric to a maximum of 4% at lean equivalence ratios.

In the test engine, a partially closed throttle plate in the individual tuned intake runner of a cylinder significantly reduced torque and intake port pressure at IVC with only a small change in intake manifold pressure. There was a strong relationship between intake manifold pressure at IVC and torque. This indicates that throttle plate disturbances significantly interfere with the torque increase due to resonance even if mean gas velocity is low and that care has been taken to minimize disturbances due to fabrication welding and intake runner bends.

Ethanol increased torque in the test engine by 5% relative to gasoline from 49.7 to 52 N*m and increased thermal efficiency from

31.1% to 33.5 % at WOT, MBT spark timing, and stoichiometric equivalence ratio. The wider flammability limit of ethanol allowed operation at the leaner equivalence ratio of .8 with a resulting increase in the maximum calculated thermal efficiency to 34.9%.

In the test engine, ethanol reduced maximum NO_x emissions by 29% from 19 g/Kw*hr to 13.5 g/kw*hr when operating near stoichiometric equivalence ratios. This can be attributed to the greater heat of vaporization of ethanol resulting in lower combustion temperatures. Specific NO_x emissions have a much higher peak for ethanol when operating at increased spark advance and equivalence ratios of .9 to .7, but specific NO_x emissions below that of gasoline can be achieved by operating at equivalence ratios below .7 with increased spark advance. Over the equivalence ratios tested for both fuels, specific HC emissions in the test engine while burning ethanol are reduced to approximately 50% of those while burning gasoline with a minimum of 2.8 g/Kw*hr achievable with ethanol at lean equivalence ratios vs. a minimum of 7.5 g/kw*hr achievable for gasoline.

CO emissions were minimized by operating at lean equivalence ratios. CO_2 emissions are approximately 63000 g/kW*hr for gasoline during stoichiometric operation at MBT spark timing. CO_2 emissions were 58000 g/kW*hr for E95 during both stoichiometric, MBT operation and at the maximum observed thermal efficiency point of 21 degrees advance and .8 equivalence ratio. This trend is expected since specific CO_2 emissions are dependent only on specific fuel consumption and fuel carbon content.

Ethanol fuel offers an alternative to the traditional operating strategy used to reduce emissions while operating on gasoline. When

using ethanol in this application, operation at an equivalence ratio of approximately .68 to .75 and a spark advance of between 10 and 21 degrees results in low BSFC and low uncatalyzed specific NOx and HC emissions. Increasing spark advance from 10 degrees to 21 degrees reduces BSFC and increases torque at the penalty of increased NOx emissions. Reducing equivalence ratio results in lower NOx emissions but also increased HC emissions and reduced torque. There is an excess of oxygen at this point, allowing easy oxidation of HC emissions if NOx emissions are already significantly lowered. Further testing in this operating region with varying spark advance may provide a better compromise than the spark advance values tested.

The higher octane rating of ethanol relative to gasoline allows E95 operation at MBT while gasoline encounters a knock limit in the test engine. Ethanol provides a larger margin of safety from knock during the severe operating conditions of WOT and stoichiometric air fuel ratio which are encountered when optimizing operation for a three way catalyst.

References

1. Whittenberger, William A., Kubsh, Joseph E. "Electrically heated metal substrate durability," S.A.E. Paper 910613, 1991.

2. Hochmuth, John K.; Bruk, Patrick L.; Tolentino, Cesar; Mignano, Michael J. "Hydrocarbon Traps for Controlling Cold Start Emissions," S.A.E. Paper 930739, 1993.

3. Michael P. Thompson, Helmuth W. Engleman. "The Two Types of Resonance in Intake Tuning," A.S.M.E. Paper 69-DGP-11, 1969.

4. Helmuth W. Engleman. "Design of a Tuned Intake Manifold," ASME Paper 73-WAA/DGP 2, 1973.

5. Heywood, John B., Internal Combustion Engine Fundamentals, McGraw Hill, New York, 1988.

6. Marks, Lionel S., Marks' Standard Handbook For Mechanical Engineers, McGraw Hill, New York, 1978.

Appendix 1
Emissions Data

Ethanol

percent CO	percent CO2	ppm HC	ppm NOX	percent O2	CYLINDER	POWER (kw)	ADVANCE
0.14	12.39	371	45	2.87	1	0.0	10
2.38	13.20	681	90	0.34	2	0.0	10
0.66	13.71	981	2616	0.97	1	17.6	10
0.32	14.13	556	3360	0.81	2	17.6	10
0.29	13.61	847	2767	1.28	1	17.2	10
0.13	13.81	519	3470	1.22	2	17.2	10
2.50	12.87	1135	1344	0.60	1	17.5	10
2.15	13.28	755	1753	0.35	2	17.5	10
1.76	13.23	1042	2137	0.70	1	0.0	21
1.60	13.63	717	2037	0.41	2	0.0	21
3.54	12.24	1182	1095	0.48	1	18.3	10
3.22	12.66	858	1265	0.26	2	18.3	10
6.37	10.68	1369	329	0.36	1	18.3	10
6.08	10.95	1080	386	0.24	2	18.3	10
0.13	12.24	867	2048	2.82	1	14.8	10
0.09	11.96	610	1762	3.15	2	14.8	10
0.11	11.22	843	653	4.00	1	13.2	10
0.09	10.99	632	699	4.28	2	13.2	10
0.13	9.94	1009	151	5.46	1	10.4	10
0.10	9.93	733	138	5.42	2	10.4	10
0.12	12.69	696	3996	2.20	1	16.1	21
0.09	12.38	497	4622	2.57	2	16.1	21
0.11	11.50	779	2775	3.63	1	15.1	21
0.09	11.26	577	2928	3.90	2	15.1	21
0.10	10.35	905	801	4.95	1	13.4	21
0.09	10.12	644	982	5.19	2	13.4	21
0.13	8.88	1384	92	6.62	1	10.2	21
0.12	8.62	1259	123	6.86	2	10.2	21

Gasoline

CO	CO2	HC	NOX	O2	CYLINDER	POWER (kW)	ADVANCE
0.50	13.69	2069	3496	1.50	1	17.3	17
0.84	13.88	1258	3731	0.92	2	17.3	17
0.95	13.45	2000	3828	1.93	1	17.0	17
0.39	13.81	1197	4361	1.41	2	17.0	17
2.56	12.67	2412	2035	0.99	1	17.6	17
2.76	12.80	1294	1860	0.58	2	17.6	17

Appendix 2
Fuel Consumption Data

Ethanol — Fuel Volume =224 ml

Average injection Pulse (microseconds) injave	spark advance	O2 sensor voltage	power (kW)	torque (N*m)	time (seconds)	coolant temp
8919	10	0.10	18.5	48.9	91.5	68
9850	10	0.88	19.6	52.0	80.0	64
9307	10	0.50	19.3	51.2	85.0	66
6974	10	0.03	10.8	28.6	118.0	73
8018	10	0.04	16.0	42.4	101.0	70
7496	10	0.04	14.1	37.4	99.5	72
10106	10	0.92	19.4	51.5	77.0	66
8592	21	0.10	18.4	48.7	91.5	65
9766	21	0.88	19.0	50.4	82.0	62
9267	21	0.50	18.9	50.1	87.0	64
6908	21	0.03	13.5	35.8	116.5	73
8018	21	0.05	17.0	45.1	100.5	74
7496	21	0.04	15.4	40.8	109.5	72
10106	21	0.92	19.0	50.4	77.0	62
gasoline						
5805	10	0.50	18.2	48.3	130.5	72
5690	10	0.10	17.9	47.5	136.5	73
5301	10	0.88	18.8	49.9	116.0	73
5994	17	0.50	18.7	49.6	128.0	68

Appendix 3
Variable Length Torque Data

RPM	18.5 inch torque (N*m)	21.5 inch torque (N*m)	24 inch torque (N*m)	27 inch torque (N*m)	Manufacturer's Manifold torque (N*m)
4000	42.7	42.7	42.2	42.0	
3800	43.8	43.8	43.5	43.6	
3600	45.6	45.4	45.8	44.8	40.5
3400	45.8	46.8	46.3	46.4	42.1
3200	47.0	47.8	47.8	47.9	43.4
3000	48.0	48.4	49.2	49.1	44.5
2800	49.0	49.1	49.0	50.0	45.3
2600	47.9	47.9	48.1	48.8	45.9
2200	45.8	46.4	46.1	46.3	46.1
2000					45.4
1800					44.5
1600					42.3

Appendix 4
Variable Spark Advance Data

Ethanol	T atm (° C)	
	25	
Advance (BTDC)	Patm(mbar)	Torque
0	1000	47.63286454
10	998	50.88741179
11	992	50.90944979
12	992	50.76846978
15	992	50.62846879
20	998	50.18415791

Gasoline	T atm (° C)	
	25	
Advance (BTDC)	Patm(mbar)	Torque
0	996	44.92198372
10	996	48.95218357
15	996	49.44367135
17	996	49.54196891
20	996	48.36239822

Appendix 5
Throttle Angle and Maniold Pressure Data for Pressure Traces

T atm (° C)	Patm (mbar)
25	1000.00

Torque	Throttle Angle	Manifold Vacuum (in Hg)
44.3	0	0.60
41.1	15	0.80
37.7	35	0.90

T atm (° C)	Patm (mbar)
25	989.00

Torque	Throttle Angle	Manifold Vacuum (in Hg)
30.5	40	1.30
22.3	55	3.05
23.9	50	2.50
16.5	75	6.65
26.3	45	2.05
34.0	25	1.00
42.7	0	0.50
0.0	90	18.00